KYBERNETIKA — VOLUME 55 (2019), NUMBER 3, PAGES 561–585

A FAMILY OF HYPERBOLIC–TYPE CONTROL SCHEMES FOR ROBOT MANIPULATORS

Fernando Reyes-Cortes, Olga Felix-Beltran, Jaime Cid-Monjaraz and Gweni Alonso-Aruffo

This paper deals with the global position control problem of robot manipulators in joint space, a new family of control schemes consisting of a suitable combination of hyperbolic functions is presented. The proposed control family includes a large class of bounded hyperbolic-type control schemes to drive both position error and derivative action terms plus gravity compensation. To ensure global asymptotic stability of closed-loop system equilibrium point, we propose an energy-shaping based strict Lyapunov function. To verify the efficiency of the proposed control algorithm, an experimental comparative analysis between the well known unbounded linear PD control and three hyperbolic-type control schemes of the proposed family on a three degrees of freedom direct-drive robot manipulator is analysed.

Keywords: Lyapunov stability, control, robot-manipulator, regulation

Classification: 68T40, 93C85, 93D05

1. INTRODUCTION

Nowadays, manipulator robots have become indispensable tools in society, for example, since the traditional applications of manipulators such as pick-and-place operations, paintings, circuit-board assembly, drilling, palletizing until space operations, physiotherapy, robotic operating rooms, and so on. These applications are basically positioning and handling devices. For a robot carry out correctly programmed tasks, a high-performance control algorithm is required; the robot manipulator performance represents an important production indicator, if the performance is high, then the exactness and productivity are increased, and this is one of the goals for every manufacturer [26, 27].

The control of robot manipulators is an area for research, development with potential applications; it is in constant growth, remains an open problem. The design of control algorithms has become a permanent and systematic scientific activity, with the purpose of proposing new control schemes of high performance for a correct execution of the programmed task. The position control problem also, so-called regulation of robot manipulators is one of the most relevant issues. It consists in to move freely in its workspace the manipulator end-effector from any initial condition to a fixed desired position, which is assumed to be constant, regardless of its initial joint position [27, 28].

DOI: 10.14736/kyb-2019-3-0561

The proportional-derivative (PD) and proportional-integral-derivative (PID) control algorithms are the most simplest regulators to achieve regulation of robot manipulators. For the case of PD control guarantees the global regulation objective [31]; while that, the PID control lacks of it, until now asymptotic stability is valid only in a local sense [13, 33]. On the other hand, there is an implicit assumption in the linear PD and PID control schemes, they are able to provide any requested joint torque, because these schemes do not incorporate input constraints from manipulator actuator limitations on their applied torques. However, due to inherent physical limitations of the robot actuators, the saturation phenomenon is always present in practical aspects when PD and PID control schemes are sufficiently large [29].

It is well known that actuators are unable to supply unlimited torques, therefore recognizing these difficulties, several control schemes that take into account these important actuator constraints have been proposed in the literature. In [24] present a fuzzy control scheme with bounded torques, it is proved the global asymptotic stability via Lyapunov theory. In [19] studies the stability properties of robot manipulators under the action of saturated PID control. A global stable nonlinear PID with saturated functions is developed in [30]; experimental results on a two robot manipulator are presented. In [1] two globally stabilizing bounded control schemes for the tracking control with saturating inputs are presented.

In [29] addresses the global asymptotic regulation under input constrains, it presents a saturated PID control in agreement with Lyapunov's direct method and LaSalle's invariance principle; the proposed approach is illustrated via simulations. In [32] a non-linear PID control with bounded torques is presented, the three terms of the regulator use a single saturation and global asymptotic stability is proved via Lyapunov stability theory; experimental results are included. In [15] based on the Lyapunov formulation a local hyperbolic-tangent-type impedance control for robot manipulators in Cartesian space is analysed; its experimental implementation of an interaction task on a two-degrees-of-freedom direct-drive robot is presented. A saturated control of a general class of uncertain non-linear systems with time-delayed actuation and additive bounded disturbances is analysed in [7]; the performance of the controller is demonstrated via simulation on a two-link planar robot manipulator. Using the theory of singularly perturbed systems, the problem of analysing a saturated PI velocity controller is addressed in [17]; an experimental study in a planar two degrees-of-freedom direct-drive robot is presented. A bounded square root-type regulator is presented in [20], the asymptotic stability is discussed via Lyapunovs direct method and LaSalle's invariance principle; experimental results on a three degrees-of-freedom direct-drive robot manipulator are presented.

In [2] considers the PD-Type control of a single-link flexible-joint manipulator subject to actuator saturation; it is shown that equilibrium point of the closed-loop system is asymptotically stable, simulation results are presented only. A saturated control for a class second-order, nonlinear systems is developed in [8], it yields asymptotic stability. The bounds on the control are known a priori and can be adjusted by changing the feedback gains; experimental results using a two-link robot manipulator are reported. Three saturated non-linear proportional-integral derivative controls with bounded torques for robot manipulators are analysed in [18], new tuning criteria on control gains to ob-

tain stability conditions, experimental tests completely fulfil the stability rules on two-degrees-of-freedom robot. A combined adaptive controller-observer system is presented in [25], which reduce the risk of actuator saturation effectively via generalized saturation functions. Semi-global uniform ultimate boundedness stability of the tracking errors and state estimation errors is obtained by Lyapunov stability; simulations results are presented. An output-feedback PID-type control for the global stabilization of robot manipulators with bounded inputs is proposed in [16], experimental tests on a two degrees-of-freedom direct-drive arm are included.

Recently, in [3] has proposed a bounded proportional control plus Hammerstein strictly positive real compensator control term to ensure that the applied torque of each servomotor is bounded by a value that is less then maximum torque, it has a asymptotically stable behavior. In [33] a PID-type control for the global regulation with constrained inputs is proposed; this controller can adopt multiple saturating structures, the global stabilization objective is guaranteed. Furthermore, experimental tests on a two degrees-of freedom are presented. In [34] a servo-constraint-based inverse dynamics control method is for under-actuated multibody systems is applied for the treatment of actuator torque saturation; numerical simulations on planar model of a acroboter service robot platform are presented. The performance of the controller is demonstrated experimentally. The work presented in [14] shows a nonlinear adaptive controller reminiscent of computed-torque-type scheme is used with saturated terms. In [21] a PD-type saturating stiffness control scheme with bounded torque inputs is presented; the corresponding local Lyapunov stability proof of the closed-loop equilibrium point is discussed. In these last two works, only simulation results are presented.

The work presented in [6] deals with control problem with high-frequency, whose joints have bounded position, velocity and acceleration/torque. It is formulated as an optimal control through the viability kernel of feasible trajectory; the used scheme is the PD control. Numerical simulations are presented on the model of Baxter robot. In [9] is addressed the problem of robust tracking control of electrically flexible joint robots through a nonlinear PID-type proposed control scheme, experimental results demonstrate high performance of the proposed control on a flexible-joint electrically driven robot.

Since the pioneering work of Takegaki and Arimoto in 1981 on energy shaping methodology with damping injection, which permits to design other control structures different from PD, it has been continued by several researchers, who have offered extensions and improvements to this methodology: [12, 20, 22, 23]. Within this context, in this paper, we propose a new family of bounded hyperbolic-type control schemes with gravity compensation for the global regulation problem of robot manipulators in joint space. The proposed control scheme is unlike other cited previously works, it is composed of a large class of hyperbolic functions, obtained by a suitable potential function to drive both the position error and damping injection, whose result produces bounded control inputs on the proportional and derivative terms, and at the same time, to deal with practical specifications such as keeping asymptotically the position error and applied torques within prescribed bounds without saturating the actuators. We provide design guidelines without regard to initial conditions to tune the controller gains, guaranteeing that the demanded torques remain inside the prescribed limits.

To the best of our knowledge, the proposed family of control algorithms is the first scheme in joint space with a suitable combination of bounded hyperbolic-type functions. The objective of this paper is to formally proof the global asymptotic stability of the closed-loop system equilibrium point, which is carried out by considering an energy shaping based strict Lyapunov function. The proposed control scheme performance resulting is experimentally evaluated and compared with those obtained for well known unbounded linear PD control algorithm with gravity compensation on a three degrees of freedom direct-drive robot. These arguments actually constitute the main motivation for this work.

This paper is organized as follows. Section 2 describes the dynamics of rigid robots and its main properties. In Section 3, states the main results of this work, the proposed family of hyperbolic-type control schemes and its global asymptotic stability proof of the closed-loop system equilibrium point is presented. Experimental results are presented in Section 4. Finally, conclusions are given in Section 5.

2. ROBOT DYNAMICS

The dynamics of a serial n-link rigid robot with viscous friction and n degrees of freedom can be written as [13, 28]:

$$\boldsymbol{\tau} \;=\; M(\boldsymbol{q})\ddot{\boldsymbol{q}} + C(\boldsymbol{q},\dot{\boldsymbol{q}})\dot{\boldsymbol{q}} + \boldsymbol{g}(\boldsymbol{q}) + B\dot{\boldsymbol{q}} \tag{1}$$

where $\boldsymbol{q}, \dot{\boldsymbol{q}}, \ddot{\boldsymbol{q}} \in \mathbb{R}^n$ are the position, velocity and acceleration joint vectors, respectively; $\boldsymbol{\tau} \in \mathbb{R}^n$ is the vector of input torques, $M(\boldsymbol{q}) \in \mathbb{R}^{n\times n}$ is the symmetric positive definite manipulator inertia matrix, $C(\boldsymbol{q},\dot{\boldsymbol{q}}) \in \mathbb{R}^{n\times n}$ is the matrix of centripetal and Coriolis torques, $\boldsymbol{g}(\boldsymbol{q}) \in \mathbb{R}^n$ is the vector of gravitational torques obtained as the gradient of the robot potential energy due to gravity and $B \in \mathbb{R}^{n\times n}$ is the positive definite diagonal matrix for the viscous friction torques, whose entries are b_{ii}, with $i = 1, 2, \ldots, n$ represent the coefficients of viscous friction for the i^{th} joint.

It is assumed that the robot links are joined together with revolute joints. Although the equation of motion (1) is complex, it has several fundamental properties which can be exploited to facilitate control system design. For the proposed controller, the following important properties are used:

Property 2.1. The matrix of inertia $M(\boldsymbol{q}) \in \mathbb{R}^{n\times n}$ is symmetric and positive definite, it satisfies:

$$\begin{aligned} M(\boldsymbol{q}) \;&=\; M^T(\boldsymbol{q});\; M(\boldsymbol{q}) > 0 \text{ and } M^{-1}(\boldsymbol{q}) > 0;\; \boldsymbol{x}^T M(\boldsymbol{q})\boldsymbol{x} > 0\; \forall \boldsymbol{q},\; \boldsymbol{x} \in \mathbb{R}^n \\ \boldsymbol{x}^T M^{-1}(\boldsymbol{q})\boldsymbol{x} \;&>\; 0\; \forall \boldsymbol{q},\; \boldsymbol{x} \in \mathbb{R}^n;\;\; M^{-1}(\boldsymbol{q}) = M^{-T}(\boldsymbol{q}) \end{aligned}$$

Property 2.2. For robots having only revolute joints, there exists a positive constant $\beta_M > 0$ such that,

$$\|M(\boldsymbol{q})\| \leq \lambda_M^{\max} < \beta_M \tag{2}$$

where $\lambda_M^{\max}$ is the eigenvalue maximum of the inertia matrix $M(\boldsymbol{q})$.

Property 2.3. If $\dot{\boldsymbol{q}} = \boldsymbol{0}$, then the centrifugal and Coriolis torques matrix $C(\boldsymbol{q},\dot{\boldsymbol{q}})$ satisfies $C(\boldsymbol{q},\boldsymbol{0}) = 0 \in \mathbb{R}^{n\times n}\;\; \forall\, \boldsymbol{q} \in \mathbb{R}^n$.

Property 2.4. The time derivative of the inertia matrix $\dot{M}(\boldsymbol{q})$ is a symmetric matrix and satisfies:

$$\dot{M}(\boldsymbol{q}) \quad = \quad C(\boldsymbol{q},\dot{\boldsymbol{q}})^T + C(\boldsymbol{q},\dot{\boldsymbol{q}}). \tag{3}$$

Property 2.5. The centrifugal and Coriolis torques matrix $C(\boldsymbol{q},\dot{\boldsymbol{q}})$ and the time derivative $\dot{M}(\boldsymbol{q})$ of the inertia matrix satisfy:

$$\frac{1}{2}\dot{\boldsymbol{q}}^T\left[\dot{M}(\boldsymbol{q}) - 2C(\boldsymbol{q},\dot{\boldsymbol{q}})\right]\dot{\boldsymbol{q}} \quad = \quad 0, \quad \forall\ \boldsymbol{q},\dot{\boldsymbol{q}} \in \mathbb{R}^n. \tag{4}$$

Thus, the matrix $\dot{M}(\boldsymbol{q}) - 2C(\boldsymbol{q},\dot{\boldsymbol{q}})$ is a skew-symmetric matrix.

Property 2.6. For robots with revolute joints, there exists a positive constant $k_c > 0$, such that

$$\|C(\boldsymbol{q},\boldsymbol{x})\boldsymbol{y}\| \quad \leq \quad k_c\|\boldsymbol{x}\|\|\boldsymbol{y}\| \ \ \forall\ \boldsymbol{q},\boldsymbol{x},\boldsymbol{y} \in \mathbb{R}^n. \tag{5}$$

Note that, $\|C(\boldsymbol{q},\dot{\boldsymbol{q}})\dot{\boldsymbol{q}}\| \leq k_c\|\dot{\boldsymbol{q}}\|^2$.

Property 2.7. The viscous friction torque $B\dot{\boldsymbol{q}}$ is a dissipate energy that satisfies: $\dot{\boldsymbol{q}}^T B\dot{\boldsymbol{q}} > 0$, $\forall \dot{\boldsymbol{q}} \neq \boldsymbol{0} \in \mathbb{R}^n$; B is a positive definite diagonal matrix, and $\lambda_B^{\min}\|\dot{\boldsymbol{q}}\|^2 \leq \dot{\boldsymbol{q}}^T B\dot{\boldsymbol{q}} \leq \lambda_B^{\max}\|\dot{\boldsymbol{q}}\|^2$, where $\lambda_B^{\min}, \lambda_B^{\max}$ are maximum and minimum eigenvalues of the viscous friction matrix B, respectively.

Property 2.8. The gravitational torque vector $\boldsymbol{g}(\boldsymbol{q})$ is bounded $\forall\ \boldsymbol{q} \in \mathbb{R}^n$ [5], there exists a constant k_g such that $\|\boldsymbol{g}(\boldsymbol{q})\| \leq k_g$, $\forall\ \boldsymbol{q} \in \mathbb{R}^n$. This also implies that, there exist positive constants $k_{gi} \in \mathbb{R}_+$, such that $|g_i(\boldsymbol{q})| \leq k_{gi}$, $i = 1, 2, \ldots, n$; where $g_i(\boldsymbol{q})$ stands for the ith element of vector $\boldsymbol{g}(\boldsymbol{q})$.

3. FAMILY OF BOUNDED HYPERBOLIC–TYPE CONTROLS

This section presents the new family of bounded hyperbolic-type control schemes and its global asymptotic stability analysis. First, we define the position control problem.

The problem of position control with bounded inputs for robot manipulators consists of to propose a control scheme such that, the applied torque $\boldsymbol{\tau} \in \mathbb{R}^n$ to robot joints be within the constrains, so that the robot joints $\boldsymbol{q}(t)$ tend asymptotically to a constant desired joint position $\boldsymbol{q}_d \in \mathbb{R}^n$, regardless the initial conditions $[\boldsymbol{q}(0),\ \dot{\boldsymbol{q}}(0)]^T \in \mathbb{R}^{2n}$, this is:

$$\lim_{t\to\infty}\begin{bmatrix}\tilde{\boldsymbol{q}}(t)\\ \dot{\boldsymbol{q}}(t)\end{bmatrix} \to \boldsymbol{0} \in \mathbb{R}^{2n},\ \forall t \geq 0$$

where $\tilde{\boldsymbol{q}} \in \mathbb{R}^n$ is the joint position error, which is defined as $\tilde{\boldsymbol{q}} = \boldsymbol{q}_d - \boldsymbol{q}(t)$.

To resolve the position control problem, we propose a control structure $\boldsymbol{\tau}$ composed by a large class of bounded hyperbolic-type functions to drive both the position error

and derivative action terms, plus gravity compensation. Consider the following family of control schemes with limited torques, given by

$$\boldsymbol{\tau} = K_p \begin{bmatrix} \frac{\sinh^{2m-1}(\tilde{q}_1)\cosh(\tilde{q}_1)}{1+\sinh^{2m}(\tilde{q}_1)} \\ \frac{\sinh^{2m-1}(\tilde{q}_2)\cosh(\tilde{q}_2)}{1+\sinh^{2m}(\tilde{q}_2)} \\ \vdots \\ \frac{\sinh^{2m-1}(\tilde{q}_n)\cosh(\tilde{q}_n)}{1+\sinh^{2m}(\tilde{q}_n)} \end{bmatrix} - K_v \begin{bmatrix} \frac{\sinh^{2m-1}(\dot{q}_1)\cosh(\dot{q}_1)}{1+\sinh^{2m}(\dot{q}_1)} \\ \frac{\sinh^{2m-1}(\dot{q}_2)\cosh(\dot{q}_2)}{1+\sinh^{2m}(\dot{q}_2)} \\ \vdots \\ \frac{\sinh^{2m-1}(\dot{q}_n)\cosh(\dot{q}_n)}{1+\sinh^{2m}(\dot{q}_n)} \end{bmatrix} + \boldsymbol{g}(\boldsymbol{q}) \tag{6}$$

where $m \in N$ is a positive integer number, $\tilde{\boldsymbol{q}}$ is the $n \times 1$ vector of joint position error; $K_p, K_v \in \mathbb{R}^{n\times n}$ are positive definite diagonal matrices, which are called proportional and derivative gains, respectively.

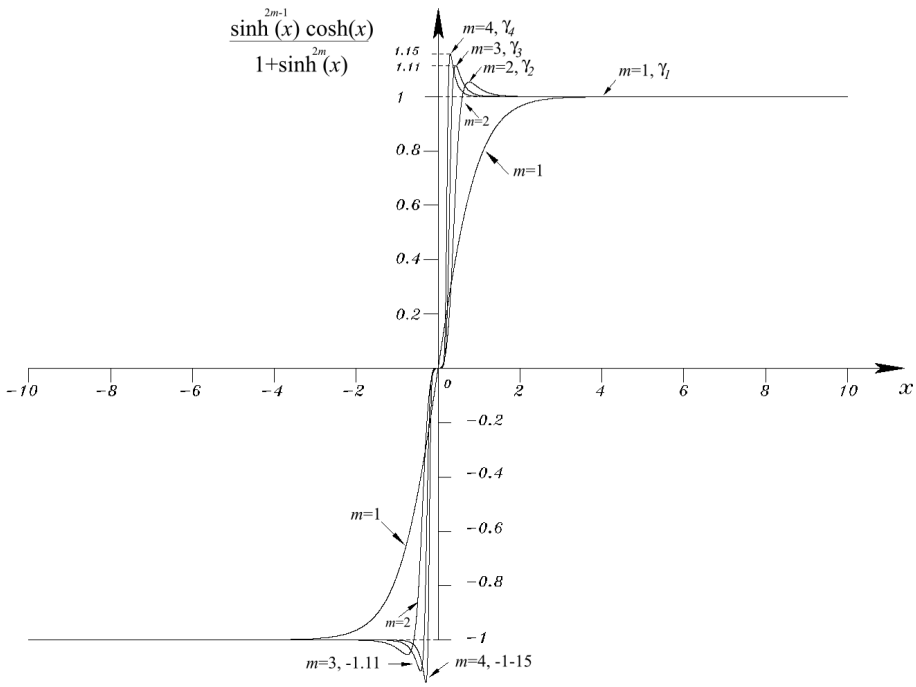

Fig. 1. Family of bounded hyperbolic functions.

The family of hyperbolic functions has a behavior as is shown in Figure 1, and satisfies

$$\left\| \begin{bmatrix} \frac{\sinh^{2m-1}(x_1)\cosh(x_1)}{1+\sinh^{2m}(x_1)} \\ \vdots \\ \frac{\sinh^{2m-1}(x_n)\cosh(x_n)}{1+\sinh^{2m}(x_n)} \end{bmatrix} \right\| \leq \begin{cases} \sqrt{n}\gamma_m, \ \forall \boldsymbol{x} \in \mathbb{R}^n \\ \sqrt{n}\gamma_m \|\boldsymbol{x}\|, \ \forall \boldsymbol{x} \in \mathbb{R}^n \end{cases} \tag{7}$$

where the number γ_m represents the upper bound (this is the peak value, and it depends on m); note that, as m increases, the slope becomes vertical; this characteristic is used

to quickly drive the position error and to obtain energy dissipation of the derivative term. The numbers γ_{p_m} and γ_{v_m} will be considered as upper bounds of the hyperbolic functions on position error and velocity, respectively.

The Euclidean norm of $\frac{\partial}{\partial \boldsymbol{x}} \frac{\sinh^{2m-1}(x_i)\cosh(x_i)}{1+\sinh^{2m}(x_)}$ with $i = 1, 2, \ldots, n$, satisfies:

$$\left\| \begin{bmatrix} \frac{\left(2m-1\right)\sinh^{2m-2}(\tilde{q}_1)+2m\sinh^{2m}(x_1)-\sinh^{4m-2}(x_1)}{\left[1+\sinh^{2m}(x_1)\right]^2} \\ \frac{\left(2m-1\right)\sinh^{2m-2}(x_2)+2m\sinh^{2m}(x_2)-\sinh^{4m-2}(x_2)}{\left[1+\sinh^{2m}(x_2)\right]^2} \\ \vdots \\ \frac{\left(2m-1\right)\sinh^{2m-2}(\tilde{q}_n)+2m\sinh^{2m}(x_n)-\sinh^{4m-2}(x_n)}{\left[1+\sinh^{2m}(x_n)\right]^2} \end{bmatrix} \right\| \leq \begin{cases} \sqrt{n}\rho_{p_m}, \ \forall \boldsymbol{x} \in \mathbb{R}^n \\ \sqrt{n}\rho_{p_m}\|\boldsymbol{x}\|, \ \forall \boldsymbol{x} \in \mathbb{R}^n \end{cases} \tag{8}$$

where ρ_{p_m} is a positive constant and represents an upper bound.

The first term of the control schemes (6) is composed by a large class of bounded hyperbolic-type regulators obtained from energy shaping of the artificial potential energy [31]. The second term acts as an hyperbolic-type damping effect on the derivative action. The control schemes (6) satisfies the following properties:

$$\|\boldsymbol{\tau}\| \quad \leq \quad \sqrt{n}\gamma_{p_m}\ \lambda_{K_p}^{\max} + \sqrt{n}\gamma_{v_m}\ \lambda_{K_v}^{\max} + k_g \leq \|\boldsymbol{\tau}^{\max}\| \tag{9}$$

where $\lambda_{K_p}^{\max}, \lambda_{K_v}^{\max}$ stand for the maximum eigenvalues of the matrices K_p and K_v, respectively; $\gamma_{p_m}, \gamma_{v_m}$ are the upper bounds for the proportional and derivative terms, respectively; and, $\|\boldsymbol{\tau}^{\max}\|$ is the Euclidean norm of allowed maximum torque vector by the robot actuators, this implies that the robot actuators are able ty supply torques in order to hold the robot at rest for all desired joint positions.

If we assume that the bounds γ_{p_m} and γ_{v_m} are equal, then we obtain a simple tuning procedure for proportional and derivative gains, given by:

$$\lambda_{K_p}^{\max} + \lambda_{K_v}^{\max} \quad \leq \quad \frac{\|\boldsymbol{\tau}^{\max}\| - k_g}{\sqrt{n}\gamma_{p_m}} \tag{10}$$

The close-loop system equation is obtained by combining the robot dynamics model (1) and the control law (6) as follows:

$$\frac{\mathrm{d}}{\mathrm{d}t}\begin{bmatrix} \tilde{\boldsymbol{q}} \\ \dot{\boldsymbol{q}} \end{bmatrix} = \begin{bmatrix} M^{-1}(\boldsymbol{q}_d - \tilde{\boldsymbol{q}}) \left[K_p \begin{bmatrix} \frac{\sinh^{2m-1}(\tilde{q}_1)\cosh(\tilde{q}_1)}{1+\sinh^{2m}(\tilde{q}_1)} \\ \frac{\sinh^{2m-1}(\tilde{q}_2)\cosh(\tilde{q}_2)}{1+\sinh^{2m}(\tilde{q}_2)} \\ \vdots \\ \frac{\sinh^{2m-1}(\tilde{q}_n)\cosh(\tilde{q}_n)}{1+\sinh^{2m}(\tilde{q}_n)} \end{bmatrix} - K_v \overset{-\dot{\boldsymbol{q}}}{\begin{bmatrix} \frac{\sinh^{2m-1}(\dot{q}_1)\cosh(\dot{q}_1)}{1+\sinh^{2m}(\dot{q}_1)} \\ \frac{\sinh^{2m-1}(\dot{q}_2)\cosh(\dot{q}_2)}{1+\sinh^{2m}(\dot{q}_2)} \\ \vdots \\ \frac{\sinh^{2m-1}(\dot{q}_n)\cosh(\dot{q}_n)}{1+\sinh^{2m}(\dot{q}_n)} \end{bmatrix}} - B\dot{\boldsymbol{q}} - C(\boldsymbol{q}_d - \tilde{\boldsymbol{q}}, \dot{\boldsymbol{q}})\dot{\boldsymbol{q}} \end{bmatrix} \tag{11}$$

which is an autonomous nonlinear differential equation.

In order to demonstrate that the state origin is the unique equilibrium point, it is necessary to consider the properties (2.1) on the matrix $M(\boldsymbol{q}_d - \tilde{\boldsymbol{q}})$ and (2.7) for the viscous friction matrix B; also, K_p, K_v are designed to be positive definite diagonal matrices. The following assumptions are taken into account:

a) The first component of the equation (11) satisfies $-\dot{\boldsymbol{q}} = -I\dot{\boldsymbol{q}} = \mathbf{0} \Leftrightarrow \dot{\boldsymbol{q}} = \mathbf{0}$, due to the fact that $I \in \mathbb{R}^{n\times n}$ is the identity matrix.

b) For the second component in the equation (11), it is easy to see that each component of the first term of bounded hyperbolic-type regulators satisfies:

$$\frac{\sinh^{2m-1}(\tilde{q}_i)\cosh(\tilde{q}_i)}{1+\sinh^{2m}(\tilde{q}_i)} = 0 \Longleftrightarrow \sinh^{2m-1}(\tilde{q}_i) = 0 \Longleftrightarrow \tilde{q}_i = 0 \implies \tilde{\boldsymbol{q}} = \mathbf{0}$$

for $i = 1, \ldots, n$; $\forall m \in N$. Similarly for the hyperbolic-derivative action term, when $\dot{\boldsymbol{q}} = \mathbf{0}$ produces a zero vector. Using the property (2.3), the vector of centripetal and Coriolis torques is the zero vector $\mathbf{0} \in \mathbb{R}^n$.

Therefore, the state origin $\left[\tilde{\boldsymbol{q}},\ \dot{\boldsymbol{q}}\right]^T = \mathbf{0} \in \mathbb{R}^{2n}$ exists and is the unique equilibrium point of the dynamics system (11).

Proposition. Consider the robot dynamics model (1) together with the control structure (6), then equilibrium point $\left[\tilde{\boldsymbol{q}},\ \dot{\boldsymbol{q}}\right]^T = \mathbf{0} \in \mathbb{R}^{2n}$ of the close-loop system (11) is globally asymptotically stable.

P r o o f. To carry out the stability analysis, we propose the following Lyapunov function candidate composed by the sum of the robot manipulator kinetic energy, artificial potential energy, plus a cross-term between position error and velocity:

$$V(\dot{\boldsymbol{q}}, \tilde{\boldsymbol{q}}) = \frac{1}{2}\dot{\boldsymbol{q}}^T M(\boldsymbol{q}_d - \tilde{\boldsymbol{q}})\dot{\boldsymbol{q}} + \frac{1}{2m}\begin{bmatrix} \sqrt{\ln\left(1+\sinh^{2m}(\tilde{q}_1)\right)} \\ \sqrt{\ln\left(1+\sinh^{2m}(\tilde{q}_2)\right)} \\ \vdots \\ \sqrt{\ln\left(1+\sinh^{2m}(\tilde{q}_n)\right)} \end{bmatrix}^T K_p \begin{bmatrix} \sqrt{\ln\left(1+\sinh^{2m}(\tilde{q}_1)\right)} \\ \sqrt{\ln\left(1+\sinh^{2m}(\tilde{q}_2)\right)} \\ \vdots \\ \sqrt{\ln\left(1+\sinh^{2m}(\tilde{q}_n)\right)} \end{bmatrix}$$

$$-\frac{\epsilon_0}{1+\|\tilde{\boldsymbol{q}}\|}\begin{bmatrix} \frac{\sinh^{2m-1}(\tilde{q}_1)\cosh(\tilde{q}_1)}{1+\sinh^{2m}(\tilde{q}_1)} \\ \frac{\sinh^{2m-1}(\tilde{q}_2)\cosh(\tilde{q}_2)}{1+\sinh^{2m}(\tilde{q}_2)} \\ \vdots \\ \frac{\sinh^{2m-1}(\tilde{q}_n)\cosh(\tilde{q}_n)}{1+\sinh^{2m}(\tilde{q}_n)} \end{bmatrix}^T M(\boldsymbol{q}_d - \tilde{\boldsymbol{q}})\dot{\boldsymbol{q}}$$

$$+\frac{1}{2}\frac{\epsilon_0^2}{\left[1+\|\tilde{\boldsymbol{q}}\|\right]^2}\begin{bmatrix}\frac{\sinh^{2m-1}(\tilde{q}_1)\cosh(\tilde{q}_1)}{1+\sinh^{2m}(\tilde{q}_1)}\\ \frac{\sinh^{2m-1}(\tilde{q}_2)\cosh(\tilde{q}_2)}{1+\sinh^{2m}(\tilde{q}_2)}\\ \vdots\\ \frac{\sinh^{2m-1}(\tilde{q}_n)\cosh(\tilde{q}_n)}{1+\sinh^{2m}(\tilde{q}_n)}\end{bmatrix}^T M(\boldsymbol{q}_d-\tilde{\boldsymbol{q}})\begin{bmatrix}\frac{\sinh^{2m-1}(\tilde{q}_1)\cosh(\tilde{q}_1)}{1+\sinh^{2m}(\tilde{q}_1)}\\ \frac{\sinh^{2m-1}(\tilde{q}_2)\cosh(\tilde{q}_2)}{1+\sinh^{2m}(\tilde{q}_2)}\\ \vdots\\ \frac{\sinh^{2m-1}(\tilde{q}_n)\cosh(\tilde{q}_n)}{1+\sinh^{2m}(\tilde{q}_n)}\end{bmatrix} \quad (12)$$

where ϵ_0 is any positive number. It is important to note the number ϵ_0 is only required for purposes of analysis, and therefore, we do not need to know its numerical value. Just it is need to prove that it exists. A strict Lyapunov function is a globally positive-definite function, whose time derivative along the trajectories of the closed-loop system (11) yields a globally negative-definite function, then Lyapunov's direct method allows to conclude global asymptotic stability, avoiding to use the Krasovskii-LaSalle theorem.

For the sake of completeness, we provide an outline of the proof that the Lyapunov function candidate (12) is a positive-definite function, note that it can be rewritten as

$$V(\dot{\boldsymbol{q}},\tilde{\boldsymbol{q}}) = \frac{1}{2}\left[\dot{\boldsymbol{q}}-\frac{\epsilon_0}{1+\|\tilde{\boldsymbol{q}}\|}\begin{bmatrix}\frac{\sinh^{2m-1}(\tilde{q}_1)\cosh(\tilde{q}_1)}{1+\sinh^{2m}(\tilde{q}_1)}\\ \frac{\sinh^{2m-1}(\tilde{q}_2)\cosh(\tilde{q}_2)}{1+\sinh^{2m}(\tilde{q}_2)}\\ \vdots\\ \frac{\sinh^{2m-1}(\tilde{q}_n)\cosh(\tilde{q}_n)}{1+\sinh^{2m}(\tilde{q}_n)}\end{bmatrix}\right]^T M(\boldsymbol{q}_d-\tilde{\boldsymbol{q}})\left[\dot{\boldsymbol{q}}-\frac{\epsilon_0}{1+\|\tilde{\boldsymbol{q}}\|}\begin{bmatrix}\frac{\sinh^{2m-1}(\tilde{q}_1)\cosh(\tilde{q}_1)}{1+\sinh^{2m}(\tilde{q}_1)}\\ \frac{\sinh^{2m-1}(\tilde{q}_2)\cosh(\tilde{q}_2)}{1+\sinh^{2m}(\tilde{q}_2)}\\ \vdots\\ \frac{\sinh^{2m-1}(\tilde{q}_n)\cosh(\tilde{q}_n)}{1+\sinh^{2m}(\tilde{q}_n)}\end{bmatrix}\right]$$

$$+\frac{1}{2m}\begin{bmatrix}\sqrt{\ln(1+\sinh^{2m}(\tilde{q}_1))}\\ \sqrt{\ln(1+\sinh^{2m}(\tilde{q}_2))}\\ \vdots\\ \sqrt{\ln(1+\sinh^{2m}(\tilde{q}_n))}\end{bmatrix}^T K_p\begin{bmatrix}\sqrt{\ln(1+\sinh^{2m}(\tilde{q}_1))}\\ \sqrt{\ln(1+\sinh^{2m}(\tilde{q}_2))}\\ \vdots\\ \sqrt{\ln(1+\sinh^{2m}(\tilde{q}_n))}\end{bmatrix}. \quad (13)$$

Since the matrix $M(\boldsymbol{q}_d-\tilde{\boldsymbol{q}})$ is a positive definite matrix, according to property (2.1), the first term of equation (13) is radially unbounded and positive-definite function in the variables $\tilde{\boldsymbol{q}}$, $\dot{\boldsymbol{q}}$ and for some $\epsilon_0 > 0$. Similarly for the second term, which is also positive definite in the variable $\tilde{\boldsymbol{q}}$, because K_p is positive definite diagonal matrix.

Now, we proceed to obtain the time derivative of the Lyapunov function candidate (12) along the trajectories of the closed-loop equation (11). Substituting the acceleration joint vector $\ddot{\boldsymbol{q}}$ from closed-loop equation (11), cancellation of some terms produce simplifications, using the property of skew-symmetric matrix (2.5) on the fourth and fifth terms; the first term is canceled with the sixth term; ninth and thirteenth terms

are cancelled using the property (2.4), we get:

$$\dot{V}(\dot{\boldsymbol{q}},\tilde{\boldsymbol{q}}) = \dot{\boldsymbol{q}}^T K_p \begin{bmatrix} \frac{\sinh^{2m-1}(\tilde{q}_1)\cosh(\tilde{q}_1)}{1+\sinh^{2m}(\tilde{q}_1)} \\ \frac{\sinh^{2m-1}(\tilde{q}_2)\cosh(\tilde{q}_2)}{1+\sinh^{2m}(\tilde{q}_2)} \\ \vdots \\ \frac{\sinh^{2m-1}(\tilde{q}_n)\cosh(\tilde{q}_n)}{1+\sinh^{2m}(\tilde{q}_n)} \end{bmatrix} \overset{\text{1 and 6}}{\nearrow} - \dot{\boldsymbol{q}}^T K_v \begin{bmatrix} \frac{\sinh^{2m-1}(\dot{q}_1)\cosh(\dot{q}_1)}{1+\sinh^{2m}(\dot{q}_1)} \\ \frac{\sinh^{2m-1}(\dot{q}_2)\cosh(\dot{q}_2)}{1+\sinh^{2m}(\dot{q}_2)} \\ \vdots \\ \frac{\sinh^{2m-1}(\dot{q}_n)\cosh(\dot{q}_n)}{1+\sinh^{2m}(\dot{q}_n)} \end{bmatrix} - \dot{\boldsymbol{q}}^T B \dot{\boldsymbol{q}}$$

$$\underbrace{-\dot{\boldsymbol{q}}^T C(\boldsymbol{q}_d-\tilde{\boldsymbol{q}},\dot{\boldsymbol{q}})\dot{\boldsymbol{q}} + \frac{1}{2}\dot{\boldsymbol{q}}^T \dot{M}(\boldsymbol{q}_d-\tilde{\boldsymbol{q}})\dot{\boldsymbol{q}}}_{\frac{1}{2}\dot{\boldsymbol{q}}^T\left[\dot{M}(\boldsymbol{q}_d-\tilde{\boldsymbol{q}})-2C(\boldsymbol{q}_d-\tilde{\boldsymbol{q}},\dot{\boldsymbol{q}})\right]\dot{\boldsymbol{q}}=0} - \dot{\boldsymbol{q}}^T K_p \begin{bmatrix} \frac{\sinh^{2m-1}(\tilde{q}_1)\cosh(\tilde{q}_1)}{1+\sinh^{2m}(\tilde{q}_1)} \\ \frac{\sinh^{2m-1}(\tilde{q}_2)\cosh(\tilde{q}_2)}{1+\sinh^{2m}(\tilde{q}_2)} \\ \vdots \\ \frac{\sinh^{2m-1}(\tilde{q}_n)\cosh(\tilde{q}_n)}{1+\sinh^{2m}(\tilde{q}_n)} \end{bmatrix} \overset{\text{1 and 6}}{\nearrow}$$

$$+\frac{\epsilon_0}{1+\|\tilde{\boldsymbol{q}}\|} \begin{bmatrix} \frac{\left[(2m-1)\sinh^{2m-2}(\tilde{q}_1)+2m\sinh^{2m}(\tilde{q}_1)-\sinh^{4m-2}(\tilde{q}_1)\right]\dot{q}_1}{\left[1+\sinh^{2m}(\tilde{q}_1)\right]^2} \\ \frac{\left[(2m-1)\sinh^{2m-2}(\tilde{q}_2)+2m\sinh^{2m}(\tilde{q}_2)-\sinh^{4m-2}(\tilde{q}_2)\right]\dot{q}_2}{\left[1+\sinh^{2m}(\tilde{q}_2)\right]^2} \\ \vdots \\ \frac{\left[(2m-1)\sinh^{2m-2}(\tilde{q}_n)+2m\sinh^{2m}(\tilde{q}_n)-\sinh^{4m-2}(\tilde{q}_n)\right]\dot{q}_n}{\left[1+\sinh^{2m}(\tilde{q}_n)\right]^2} \end{bmatrix}^T M(\boldsymbol{q}_d-\tilde{\boldsymbol{q}})\dot{\boldsymbol{q}}$$

$$-\frac{\epsilon_0 \tilde{\boldsymbol{q}}^T\dot{\boldsymbol{q}}}{\|\tilde{\boldsymbol{q}}\|\left[1+\|\tilde{\boldsymbol{q}}\|\right]^2} \begin{bmatrix} \frac{\sinh^{2m-1}(\tilde{q}_1)\cosh(\tilde{q}_1)}{1+\sinh^{2m}(\tilde{q}_1)} \\ \frac{\sinh^{2m-1}(\tilde{q}_2)\cosh(\tilde{q}_2)}{1+\sinh^{2m}(\tilde{q}_2)} \\ \vdots \\ \frac{\sinh^{2m-1}(\tilde{q}_n)\cosh(\tilde{q}_n)}{1+\sinh^{2m}(\tilde{q}_n)} \end{bmatrix}^T M(\boldsymbol{q}_d-\tilde{\boldsymbol{q}})\dot{\boldsymbol{q}}$$

$$-\frac{\epsilon_0}{1+\|\tilde{\boldsymbol{q}}\|} \begin{bmatrix} \frac{\sinh^{2m-1}(\tilde{q}_1)\cosh(\tilde{q}_1)}{1+\sinh^{2m}(\tilde{q}_1)} \\ \frac{\sinh^{2m-1}(\tilde{q}_2)\cosh(\tilde{q}_2)}{1+\sinh^{2m}(\tilde{q}_2)} \\ \vdots \\ \frac{\sinh^{2m-1}(\tilde{q}_n)\cosh(\tilde{q}_n)}{1+\sinh^{2m}(\tilde{q}_n)} \end{bmatrix}^T \underbrace{\left[C(\boldsymbol{q}_d-\tilde{\boldsymbol{q}},\dot{\boldsymbol{q}}) \overset{\text{9 and 13}}{\nearrow} + C(\boldsymbol{q}_d-\tilde{\boldsymbol{q}},\dot{\boldsymbol{q}})^T\right]\dot{\boldsymbol{q}}}_{\dot{M}(\boldsymbol{q}_d-\tilde{\boldsymbol{q}})}$$

$$-\frac{\epsilon_0}{1+\|\tilde{\boldsymbol{q}}\|} \begin{bmatrix} \frac{\sinh^{2m-1}(\tilde{q}_1)\cosh(\tilde{q}_1)}{1+\sinh^{2m}(\tilde{q}_1)} \\ \frac{\sinh^{2m-1}(\tilde{q}_2)\cosh(\tilde{q}_2)}{1+\sinh^{2m}(\tilde{q}_2)} \\ \vdots \\ \frac{\sinh^{2m-1}(\tilde{q}_n)\cosh(\tilde{q}_n)}{1+\sinh^{2m}(\tilde{q}_n)} \end{bmatrix}^T K_p \begin{bmatrix} \frac{\sinh^{2m-1}(\tilde{q}_1)\cosh(\tilde{q}_1)}{1+\sinh^{2m}(\tilde{q}_1)} \\ \frac{\sinh^{2m-1}(\tilde{q}_2)\cosh(\tilde{q}_2)}{1+\sinh^{2m}(\tilde{q}_2)} \\ \vdots \\ \frac{\sinh^{2m-1}(\tilde{q}_n)\cosh(\tilde{q}_n)}{1+\sinh^{2m}(\tilde{q}_n)} \end{bmatrix} + \frac{\epsilon_0}{1+\|\tilde{\boldsymbol{q}}\|} \begin{bmatrix} \frac{\sinh^{2m-1}(\tilde{q}_1)\cosh(\tilde{q}_1)}{1+\sinh^{2m}(\tilde{q}_1)} \\ \frac{\sinh^{2m-1}(\tilde{q}_2)\cosh(\tilde{q}_2)}{1+\sinh^{2m}(\tilde{q}_2)} \\ \vdots \\ \frac{\sinh^{2m-1}(\tilde{q}_n)\cosh(\tilde{q}_n)}{1+\sinh^{2m}(\tilde{q}_n)} \end{bmatrix}^T B\dot{\boldsymbol{q}}$$

$$+\frac{\epsilon_0}{1+\|\tilde{\boldsymbol{q}}\|} \begin{bmatrix} \frac{\sinh^{2m-1}(\tilde{q}_1)\cosh(\tilde{q}_1)}{1+\sinh^{2m}(\tilde{q}_1)} \\ \frac{\sinh^{2m-1}(\tilde{q}_2)\cosh(\tilde{q}_2)}{1+\sinh^{2m}(\tilde{q}_2)} \\ \vdots \\ \frac{\sinh^{2m-1}(\tilde{q}_n)\cosh(\tilde{q}_n)}{1+\sinh^{2m}(\tilde{q}_n)} \end{bmatrix}^T K_v \begin{bmatrix} \frac{\sinh^{2m-1}(\dot{q}_1)\cosh(\dot{q}_1)}{1+\sinh^{2m}(\dot{q}_1)} \\ \frac{\sinh^{2m-1}(\dot{q}_2)\cosh(\dot{q}_2)}{1+\sinh^{2m}(\dot{q}_2)} \\ \vdots \\ \frac{\sinh^{2m-1}(\dot{q}_n)\cosh(\dot{q}_n)}{1+\sinh^{2m}(\dot{q}_n)} \end{bmatrix}$$

$$
\begin{aligned}
&+\frac{\epsilon_0}{1+\|\tilde{\boldsymbol{q}}\|}\begin{bmatrix}\frac{\sinh^{2m-1}(\tilde{q}_1)\cosh(\tilde{q}_1)}{1+\sinh^{2m}(\tilde{q}_1)}\\ \frac{\sinh^{2m-1}(\tilde{q}_2)\cosh(\tilde{q}_2)}{1+\sinh^{2m}(\tilde{q}_2)}\\ \vdots\\ \frac{\sinh^{2m-1}(\tilde{q}_n)\cosh(\tilde{q}_n)}{1+\sinh^{2m}(\tilde{q}_n)}\end{bmatrix}^T \underbrace{C(\boldsymbol{q}_d-\tilde{\boldsymbol{q}},\dot{\boldsymbol{q}})\dot{\boldsymbol{q}}}_{9 \text{ and } 13}\\
&+\frac{1}{2}\frac{\epsilon_0^2}{\left[1+\|\tilde{\boldsymbol{q}}\|\right]^2}\begin{bmatrix}\frac{\sinh^{2m-1}(\tilde{q}_1)\cosh(\tilde{q}_1)}{1+\sinh^{2m}(\tilde{q}_1)}\\ \frac{\sinh^{2m-1}(\tilde{q}_2)\cosh(\tilde{q}_2)}{1+\sinh^{2m}(\tilde{q}_2)}\\ \vdots\\ \frac{\sinh^{2m-1}(\tilde{q}_n)\cosh(\tilde{q}_n)}{1+\sinh^{2m}(\tilde{q}_n)}\end{bmatrix}^T \begin{bmatrix}\underbrace{C(\boldsymbol{q}_d-\tilde{\boldsymbol{q}},\dot{\boldsymbol{q}})+C(\boldsymbol{q}_d-\tilde{\boldsymbol{q}},\dot{\boldsymbol{q}})^T}_{\dot{M}(\boldsymbol{q}_d-\tilde{\boldsymbol{q}})}\end{bmatrix} \begin{bmatrix}\frac{\sinh^{2m-1}(\tilde{q}_1)\cosh(\tilde{q}_1)}{1+\sinh^{2m}(\tilde{q}_1)}\\ \frac{\sinh^{2m-1}(\tilde{q}_2)\cosh(\tilde{q}_2)}{1+\sinh^{2m}(\tilde{q}_2)}\\ \vdots\\ \frac{\sinh^{2m-1}(\tilde{q}_n)\cosh(\tilde{q}_n)}{1+\sinh^{2m}(\tilde{q}_n)}\end{bmatrix}\\
&+\frac{1}{2}\frac{\epsilon_0^2}{\left[1+\|\tilde{\boldsymbol{q}}\|\right]^2}\begin{bmatrix}\frac{\sinh^{2m-1}(\tilde{q}_1)\cosh(\tilde{q}_1)}{1+\sinh^{2m}(\tilde{q}_1)}\\ \frac{\sinh^{2m-1}(\tilde{q}_2)\cosh(\tilde{q}_2)}{1+\sinh^{2m}(\tilde{q}_2)}\\ \vdots\\ \frac{\sinh^{2m-1}(\tilde{q}_n)\cosh(\tilde{q}_n)}{1+\sinh^{2m}(\tilde{q}_n)}\end{bmatrix}^T \frac{2\tilde{\boldsymbol{q}}^T\dot{\boldsymbol{q}}}{\|\tilde{\boldsymbol{q}}\|\left[1+\|\tilde{\boldsymbol{q}}\|\right]}M(\boldsymbol{q}_d-\tilde{\boldsymbol{q}}) \begin{bmatrix}\frac{\sinh^{2m-1}(\tilde{q}_1)\cosh(\tilde{q}_1)}{1+\sinh^{2m}(\tilde{q}_1)}\\ \frac{\sinh^{2m-1}(\tilde{q}_2)\cosh(\tilde{q}_2)}{1+\sinh^{2m}(\tilde{q}_2)}\\ \vdots\\ \frac{\sinh^{2m-1}(\tilde{q}_n)\cosh(\tilde{q}_n)}{1+\sinh^{2m}(\tilde{q}_n)}\end{bmatrix}\\
&-\frac{\epsilon_0^2}{\left[1+\|\tilde{\boldsymbol{q}}\|\right]^2}\begin{bmatrix}\frac{\left[(2m-1)\sinh^{2m-2}(\tilde{q}_1)+2m\sinh^{2m}(\tilde{q}_1)-\sinh^{4m-2}(\tilde{q}_1)\right]\dot{q}_1}{\left[1+\sinh^{2m}(\tilde{q}_1)\right]^2}\\ \frac{\left[(2m-1)\sinh^{2m-2}(\tilde{q}_2)+2m\sinh^{2m}(\tilde{q}_2)-\sinh^{4m-2}(\tilde{q}_2)\right]\dot{q}_2}{\left[1+\sinh^{2m}(\tilde{q}_2)\right]^2}\\ \vdots\\ \frac{\left[(2m-1)\sinh^{2m-2}(\tilde{q}_n)+2m\sinh^{2m}(\tilde{q}_n)-\sinh^{4m-2}(\tilde{q}_n)\right]\dot{q}_n}{\left[1+\sinh^{2m}(\tilde{q}_n)\right]^2}\end{bmatrix}^T M(\boldsymbol{q}_d-\tilde{\boldsymbol{q}}) \begin{bmatrix}\frac{\sinh^{2m-1}(\tilde{q}_1)\cosh(\tilde{q}_1)}{1+\sinh^{2m}(\tilde{q}_1)}\\ \frac{\sinh^{2m-1}(\tilde{q}_2)\cosh(\tilde{q}_2)}{1+\sinh^{2m}(\tilde{q}_2)}\\ \vdots\\ \frac{\sinh^{2m-1}(\tilde{q}_n)\cosh(\tilde{q}_n)}{1+\sinh^{2m}(\tilde{q}_n)}\end{bmatrix}
\end{aligned}
\tag{14}
$$

Considering the above simplifications, $\dot{V}(\dot{\boldsymbol{q}},\tilde{\boldsymbol{q}})$ takes the form:

$$
\begin{aligned}
\dot{V}(\dot{\boldsymbol{q}},\tilde{\boldsymbol{q}}) \;=\; & -\dot{\boldsymbol{q}}^T K_v \begin{bmatrix}\frac{\sinh^{2m-1}(\dot{q}_1)\cosh(\dot{q}_1)}{1+\sinh^{2m}(\dot{q}_1)}\\ \frac{\sinh^{2m-1}(\dot{q}_2)\cosh(\dot{q}_2)}{1+\sinh^{2m}(\dot{q}_2)}\\ \vdots\\ \frac{\sinh^{2m-1}(\dot{q}_n)\cosh(\dot{q}_n)}{1+\sinh^{2m}(\dot{q}_n)}\end{bmatrix} - \dot{\boldsymbol{q}}^T B\dot{\boldsymbol{q}}\\
& +\frac{\epsilon_0}{1+\|\tilde{\boldsymbol{q}}\|}\begin{bmatrix}\frac{\left[(2m-1)\sinh^{2m-2}(\tilde{q}_1)+2m\sinh^{2m}(\tilde{q}_1)-\sinh^{4m-2}(\tilde{q}_1)\right]\dot{q}_1}{\left[1+\sinh^{2m}(\tilde{q}_1)\right]^2}\\ \frac{\left[(2m-1)\sinh^{2m-2}(\tilde{q}_2)+2m\sinh^{2m}(\tilde{q}_2)-\sinh^{4m-2}(\tilde{q}_2)\right]\dot{q}_2}{\left[1+\sinh^{2m}(\tilde{q}_2)\right]^2}\\ \vdots\\ \frac{\left[(2m-1)\sinh^{2m-2}(\tilde{q}_n)+2m\sinh^{2m}(\tilde{q}_n)-\sinh^{4m-2}(\tilde{q}_n)\right]\dot{q}_n}{\left[1+\sinh^{2m}(\tilde{q}_n)\right]^2}\end{bmatrix}^T M(\boldsymbol{q}_d-\tilde{\boldsymbol{q}})\dot{\boldsymbol{q}}\\
& -\frac{\epsilon_0\tilde{\boldsymbol{q}}^T\dot{\boldsymbol{q}}}{\|\tilde{\boldsymbol{q}}\|\left[1+\|\tilde{\boldsymbol{q}}\|\right]^2}\begin{bmatrix}\frac{\sinh^{2m-1}(\tilde{q}_1)\cosh(\tilde{q}_1)}{1+\sinh^{2m}(\tilde{q}_1)}\\ \frac{\sinh^{2m-1}(\tilde{q}_2)\cosh(\tilde{q}_2)}{1+\sinh^{2m}(\tilde{q}_2)}\\ \vdots\\ \frac{\sinh^{2m-1}(\tilde{q}_n)\cosh(\tilde{q}_n)}{1+\sinh^{2m}(\tilde{q}_n)}\end{bmatrix}^T M(\boldsymbol{q}_d-\tilde{\boldsymbol{q}})\dot{\boldsymbol{q}} - \frac{\epsilon_0}{1+\|\tilde{\boldsymbol{q}}\|}\begin{bmatrix}\frac{\sinh^{2m-1}(\tilde{q}_1)\cosh(\tilde{q}_1)}{1+\sinh^{2m}(\tilde{q}_1)}\\ \frac{\sinh^{2m-1}(\tilde{q}_2)\cosh(\tilde{q}_2)}{1+\sinh^{2m}(\tilde{q}_2)}\\ \vdots\\ \frac{\sinh^{2m-1}(\tilde{q}_n)\cosh(\tilde{q}_n)}{1+\sinh^{2m}(\tilde{q}_n)}\end{bmatrix}^T C(\boldsymbol{q}_d-\tilde{\boldsymbol{q}},\dot{\boldsymbol{q}})^T\dot{\boldsymbol{q}}
\end{aligned}
$$

$$
-\frac{\epsilon_0}{1+\|\tilde{\boldsymbol{q}}\|}\begin{bmatrix}\frac{\sinh^{2m-1}(\tilde{q}_1)\cosh(\tilde{q}_1)}{1+\sinh^{2m}(\tilde{q}_1)}\\ \frac{\sinh^{2m-1}(\tilde{q}_2)\cosh(\tilde{q}_2)}{1+\sinh^{2m}(\tilde{q}_2)}\\ \vdots\\ \frac{\sinh^{2m-1}(\tilde{q}_n)\cosh(\tilde{q}_n)}{1+\sinh^{2m}(\tilde{q}_n)}\end{bmatrix}^T K_p \begin{bmatrix}\frac{\sinh^{2m-1}(\tilde{q}_1)\cosh(\tilde{q}_1)}{1+\sinh^{2m}(\tilde{q}_1)}\\ \frac{\sinh^{2m-1}(\tilde{q}_2)\cosh(\tilde{q}_2)}{1+\sinh^{2m}(\tilde{q}_2)}\\ \vdots\\ \frac{\sinh^{2m-1}(\tilde{q}_n)\cosh(\tilde{q}_n)}{1+\sinh^{2m}(\tilde{q}_n)}\end{bmatrix} + \frac{\epsilon_0}{1+\|\tilde{\boldsymbol{q}}\|}\begin{bmatrix}\frac{\sinh^{2m-1}(\tilde{q}_1)\cosh(\tilde{q}_1)}{1+\sinh^{2m}(\tilde{q}_1)}\\ \frac{\sinh^{2m-1}(\tilde{q}_2)\cosh(\tilde{q}_2)}{1+\sinh^{2m}(\tilde{q}_2)}\\ \vdots\\ \frac{\sinh^{2m-1}(\tilde{q}_n)\cosh(\tilde{q}_n)}{1+\sinh^{2m}(\tilde{q}_n)}\end{bmatrix}^T B\dot{\boldsymbol{q}}
$$

$$
+\frac{\epsilon_0}{1+\|\tilde{\boldsymbol{q}}\|}\begin{bmatrix}\frac{\sinh^{2m-1}(\tilde{q}_1)\cosh(\tilde{q}_1)}{1+\sinh^{2m}(\tilde{q}_1)}\\ \frac{\sinh^{2m-1}(\tilde{q}_2)\cosh(\tilde{q}_2)}{1+\sinh^{2m}(\tilde{q}_2)}\\ \vdots\\ \frac{\sinh^{2m-1}(\tilde{q}_n)\cosh(\tilde{q}_n)}{1+\sinh^{2m}(\tilde{q}_n)}\end{bmatrix}^T K_v \begin{bmatrix}\frac{\sinh^{2m-1}(\dot{q}_1)\cosh(\dot{q}_1)}{1+\sinh^{2m}(\dot{q}_1)}\\ \frac{\sinh^{2m-1}(\dot{q}_2)\cosh(\dot{q}_2)}{1+\sinh^{2m}(\dot{q}_2)}\\ \vdots\\ \frac{\sinh^{2m-1}(\dot{q}_n)\cosh(\dot{q}_n)}{1+\sinh^{2m}(\dot{q}_n)}\end{bmatrix}
$$

$$
+\frac{1}{2}\frac{\epsilon_0^2}{\left[1+\|\tilde{\boldsymbol{q}}\|\right]^2}\begin{bmatrix}\frac{\sinh^{2m-1}(\tilde{q}_1)\cosh(\tilde{q}_1)}{1+\sinh^{2m}(\tilde{q}_1)}\\ \frac{\sinh^{2m-1}(\tilde{q}_2)\cosh(\tilde{q}_2)}{1+\sinh^{2m}(\tilde{q}_2)}\\ \vdots\\ \frac{\sinh^{2m-1}(\tilde{q}_n)\cosh(\tilde{q}_n)}{1+\sinh^{2m}(\tilde{q}_n)}\end{bmatrix}^T \left[C(\boldsymbol{q}_d-\tilde{\boldsymbol{q}},\dot{\boldsymbol{q}})+C(\boldsymbol{q}_d-\tilde{\boldsymbol{q}},\dot{\boldsymbol{q}})^T\right] \begin{bmatrix}\frac{\sinh^{2m-1}(\tilde{q}_1)\cosh(\tilde{q}_1)}{1+\sinh^{2m}(\tilde{q}_1)}\\ \frac{\sinh^{2m-1}(\tilde{q}_2)\cosh(\tilde{q}_2)}{1+\sinh^{2m}(\tilde{q}_2)}\\ \vdots\\ \frac{\sinh^{2m-1}(\tilde{q}_n)\cosh(\tilde{q}_n)}{1+\sinh^{2m}(\tilde{q}_n)}\end{bmatrix}
$$

$$
+\frac{\epsilon_0^2}{[1+\|\tilde{\boldsymbol{q}}\|]^2}\begin{bmatrix}\frac{\sinh^{2m-1}(\tilde{q}_1)\cosh(\tilde{q}_1)}{1+\sinh^{2m}(\tilde{q}_1)}\\ \frac{\sinh^{2m-1}(\tilde{q}_2)\cosh(\tilde{q}_2)}{1+\sinh^{2m}(\tilde{q}_2)}\\ \vdots\\ \frac{\sinh^{2m-1}(\tilde{q}_n)\cosh(\tilde{q}_n)}{1+\sinh^{2m}(\tilde{q}_n)}\end{bmatrix}^T \frac{\tilde{\boldsymbol{q}}^T\dot{\boldsymbol{q}}}{\|\tilde{\boldsymbol{q}}\|\left[1+\|\tilde{\boldsymbol{q}}\|\right]} M(\boldsymbol{q}_d-\tilde{\boldsymbol{q}}) \begin{bmatrix}\frac{\sinh^{2m-1}(\tilde{q}_1)\cosh(\tilde{q}_1)}{1+\sinh^{2m}(\tilde{q}_1)}\\ \frac{\sinh^{2m-1}(\tilde{q}_2)\cosh(\tilde{q}_2)}{1+\sinh^{2m}(\tilde{q}_2)}\\ \vdots\\ \frac{\sinh^{2m-1}(\tilde{q}_n)\cosh(\tilde{q}_n)}{1+\sinh^{2m}(\tilde{q}_n)}\end{bmatrix}
$$

$$
-\frac{\epsilon_0^2}{[1+\|\tilde{\boldsymbol{q}}\|]^2}\begin{bmatrix}\frac{\left[(2m-1)\sinh^{2m-2}(\tilde{q}_1)+2m\sinh^{2m}(\tilde{q}_1)-\sinh^{4m-2}(\tilde{q}_1)\right]\dot{q}_1}{\left[1+\sinh^{2m}(\tilde{q}_1)\right]^2}\\ \frac{\left[(2m-1)\sinh^{2m-2}(\tilde{q}_2)+2m\sinh^{2m}(\tilde{q}_2)-\sinh^{4m-2}(\tilde{q}_2)\right]\dot{q}_2}{\left[1+\sinh^{2m}(\tilde{q}_2)\right]^2}\\ \vdots\\ \frac{\left[(2m-1)\sinh^{2m-2}(\tilde{q}_n)+2m\sinh^{2m}(\tilde{q}_n)-\sinh^{4m-2}(\tilde{q}_n)\right]\dot{q}_n}{\left[1+\sinh^{2m}(\tilde{q}_n)\right]^2}\end{bmatrix}^T M(\boldsymbol{q}_d-\tilde{\boldsymbol{q}}) \begin{bmatrix}\frac{\sinh^{2m-1}(\tilde{q}_1)\cosh(\tilde{q}_1)}{1+\sinh^{2m}(\tilde{q}_1)}\\ \frac{\sinh^{2m-1}(\tilde{q}_2)\cosh(\tilde{q}_2)}{1+\sinh^{2m}(\tilde{q}_2)}\\ \vdots\\ \frac{\sinh^{2m-1}(\tilde{q}_n)\cosh(\tilde{q}_n)}{1+\sinh^{2m}(\tilde{q}_n)}\end{bmatrix} \tag{15}
$$

Now, we provide upper bounds on all terms of Lyapunov function, on the right-hand side of the expression (15), we use the inequalities (7) and (8), together with the properties (2.2), (2.6), and (2.7). After performing algebraic cancellation and reduction of terms, we obtain:

$$
\begin{aligned}
\dot{V}(\dot{\boldsymbol{q}},\tilde{\boldsymbol{q}} &\leq -\frac{\epsilon_0}{1+\|\tilde{\boldsymbol{q}}\|}n\gamma_{p_m}^2\lambda_{K_p}^{\min}\|\tilde{\boldsymbol{q}}\|^2\\
&-\left[\lambda_B^{\min}-\sqrt{n}\left[\gamma_{v_m}\lambda_{K_v}^{\max}+\frac{\epsilon_0}{1+\|\tilde{\boldsymbol{q}}\|}\left(\beta_M\left(\rho_{p_m}+\gamma_{p_m}\right)+\gamma_{p_m}k_c\right)\right]\right]\|\dot{\boldsymbol{q}}\|^2\\
&+\frac{\epsilon_0}{1+\|\tilde{\boldsymbol{q}}\|}\left[\sqrt{n}\gamma_{p_m}\lambda_B^{\max}+n\rho_{p_m}\gamma_{v_m}\lambda_{K_v}^{\max}+n\gamma_{p_m}\epsilon_0\left(\gamma_{p_m}k_c+\beta_M\left(\gamma_{p_m}+\rho_{p_m}\right)\right)\right]\|\tilde{\boldsymbol{q}}\|\|\dot{\boldsymbol{q}}\|
\end{aligned}
$$

$$\dot{V}(\dot{\boldsymbol{q}},\tilde{\boldsymbol{q}}) \;\leq\; -\begin{bmatrix}\|\tilde{\boldsymbol{q}}\|\\ \|\dot{\boldsymbol{q}}\|\end{bmatrix}^{T}\underbrace{\begin{bmatrix}\theta_{11} & \theta_{12}\\ \theta_{21} & \theta_{22}\end{bmatrix}}_{\Theta}\begin{bmatrix}\|\tilde{\boldsymbol{q}}\|\\ \|\dot{\boldsymbol{q}}\|\end{bmatrix} < 0 \tag{16}$$

where

$$\begin{aligned}
\theta_{11} &= \frac{\epsilon_0}{1+\|\tilde{\boldsymbol{q}}\|}n\gamma_{p_m}^2\lambda_{K_p}^{\min}\\
\theta_{12} &= \theta_{21} = -\frac{1}{2}\,\frac{\epsilon_0}{1+\|\tilde{\boldsymbol{q}}\|}\left[\sqrt{n}\gamma_{p_m}\lambda_B^{\max}+n\rho_{p_m}\gamma_{v_m}\lambda_{K_v}^{\max}+n\gamma_{p_m}\epsilon_0\left(\gamma_{p_m}k_c+\beta_M\left(\gamma_{p_m}+\rho_{p_m}\right)\right)\right]\\
\theta_{22} &= \lambda_B^{\min}-\sqrt{n}\left[\gamma_{v_m}\lambda_{K_v}^{\max}+\tfrac{\epsilon_0}{1+\|\tilde{\boldsymbol{q}}\|}\left(\beta_M\left(\rho_{p_m}+\gamma_{p_m}\right)+\gamma_{p_m}k_c\right)\right].
\end{aligned}$$

In order to ensure that Θ be a positive definite matrix, the element q_{11} is positive due to that the constants $\epsilon_0, n, \gamma_{p_m}, \lambda_{K_p}^{\min}$ all are positive numbers. The determinant $\det[\Theta]$ of the matrix Θ must be positive, this condition is satisfied for any ϵ_0 on the next interval:

$$\begin{aligned}
n\gamma_{m_p}^2\lambda_{K_p}^{\min}\left[\lambda_B^{\min}-\sqrt{n}\gamma_{m_v}\lambda_{K_v}^{\max}\right] &> \frac{\epsilon_0}{1+\|\tilde{\boldsymbol{q}}\|}\Big[n\gamma_{m_p}^2\lambda_{K_p}^{\min}\left[\beta_M\left(\rho_{m_p}+\gamma_{m_p}\right)+\gamma_{m_p}k_c\right]\\
&\quad+\frac{1}{4}\,\Big[\sqrt{n}\gamma_{m_p}\lambda_B^{\max}+n\rho_{m_p}\gamma_{m_v}\lambda_{K_v}^{\max}\\
&\qquad+n\gamma_{m_p}\epsilon_0\left(\gamma_{m_p}k_c+\beta_M\left(\gamma_{m_p}+\rho_{m_p}\right)\right)\Big]^2\Big] > 0\\
&> \frac{\epsilon_0}{1+\|\tilde{\boldsymbol{q}}\|}\Big[n\gamma_{m_p}^2\lambda_{K_p}^{\min}\left[\beta_M\left(\rho_{m_p}+\gamma_{m_p}\right)+\gamma_{m_p}k_c\right]\\
&\quad+\frac{1}{4}\,\left[\sqrt{n}\gamma_{m_p}\lambda_B^{\max}+n\rho_{m_p}\gamma_{m_v}\lambda_{K_v}^{\max}\right]^2\Big] > 0. \qquad (17)
\end{aligned}$$

Therefore, the positive number ϵ_0 exists on the interval:

$$\frac{n\gamma_{m_p}^2\lambda_{K_p}^{\min}\left[\lambda_B^{\min}-\sqrt{n}\gamma_{m_v}\lambda_{K_v}^{\max}\right]}{n\gamma_{m_p}^2\lambda_{K_p}^{\min}\left[\beta_M\left(\rho_{m_p}+\gamma_{m_p}\right)+\gamma_{m_p}k_c\right]+\frac{1}{4}\,\left[\sqrt{n}\gamma_{m_p}\lambda_B^{\max}+n\rho_{m_p}\gamma_{m_v}\lambda_{K_v}^{\max}\right]^2} > \frac{\epsilon_0}{1+\|\tilde{\boldsymbol{q}}\|} > 0. \tag{18}$$

Observe, from inequality (18) is only sufficient to hold for any ϵ_0 the next condition:

$$\frac{\lambda_B^{\min}}{\sqrt{n}\gamma_{m_v}} \;>\; \lambda_{K_v}^{\max} > 0 \tag{19}$$

which completes the proof. □

We can conclude that $\dot{V}(\dot{\boldsymbol{q}},\tilde{\boldsymbol{q}})$ is a negative definite function, due to the fact that both conditions $V(\dot{\boldsymbol{q}},\tilde{\boldsymbol{q}}) > 0$ and $\dot{V}(\dot{\boldsymbol{q}},\tilde{\boldsymbol{q}}) < 0$ are satisfied, then the proposed Lyapunov function candidate is a strict Lyapunov function. Therefore, according to Lyapunov's direct method, we conclude asymptotic stability of the origin $\left[\tilde{\boldsymbol{q}},\dot{\boldsymbol{q}}\right]^T = \mathbf{0} \in \mathbb{R}^{2n}$ of the closed-loop equation (11), this means that both state variables $\tilde{\boldsymbol{q}}(t)$ and $\dot{\boldsymbol{q}}(t)$ asymptotically converge to zero, as $t \longrightarrow \infty$.

4. EXPERIMENTAL RESULTS

To support our theoretical developments, this Section describes the robot manipulator setup and the experimental results of the proposed control schemes. An experimental system for research of robot control algorithms has been designed and built at The Benemérita Universidad Autónoma de Puebla, México; it is an anthropomorphic arm with three degrees of freedom moving in three-dimensional space, whose length of the links is 0.45 m, and workspace is a sphere with radius of 1 m, as it is shown in Figure 4. The arm links are made of 6061 aluminium actuated by brushless direct-drive servomotors from Parker Compumotor to drive the robot joints without gear reduction. Advantages of this type of direct-drive actuators include freedom from backslash, significantly lower friction phenomena compared with actuators composed by gear drives, and they work as an ideal source of applied torque. The servomotor models used in the experimental robot are listed in Table I.

Fig. 2. Experimental robot manipulator

Link	Model	Torque [Nm]	Enconder [p/rev]
Base	DM1050A	50	1024000
Shoulder	DM1150A	150	1024000
Elbow	DM1015B	15	655360

Tab. 1. Servo actuators of the experimental robot.

All the servomotors are operated in torque mode, so they act as a torque source, accepting an analogue voltage input as a reference of torque signal. Position information is obtained from incremental encoders located within the motors. The standard

backwards difference algorithm applied to the position joint measurements was used to generate the velocity signals. The electronic interface of the robot manipulator is composed by a motion control board, it is the MFIO-3A model manufactured by Precision MicroDynamic Inc., the evaluated control algorithms have been written en C language, and the sampling rate is executed at 2.5 ms on a Pentium III host computer: "the selected sampling period is less than 10% of the step response settling time for adequate recognition of the system dynamics [10]". With reference to our direct-drive robot, only the gravitational vector is required to implement the new family of controllers (6), which is available in [4].

We present an experimental comparison among three hyperbolic-type controllers versus the simple proportional-derivative (PD) controller. To investigate the performance among controllers on a direct–drive robot arm, they have been classified as $\tau_{m1},\ \tau_{m2},\ \tau_{m3}$ for the hyperbolic-type controllers with exponent $m = 1$, $m = 2$ and $m = 3$, respectively; and, τ_{PD} represents the popular PD control. The scalar–valued $\mathcal{L}^2$ norm is used to measure the performance of control algorithms. A small $\mathcal{L}^2$ norm represents smaller position error and thus is the better performance [20].

The experiment consists of moving the manipulator end–effector from its initial position to a fixed desired target. All the evaluated controllers did not show any type of friction compensation. Extensive experiments were carried out with the proposed control algorithms, however due to lack of space, we only present the corresponding results for the desired joint positions: $[q_{d1}, q_{d2}, q_{d3}]^T = [45,\ 45,\ 90]^T$ degrees, which represent the base, shoulder, and elbow joints, respectively. The initial positions and velocities were set to zero for example, at home position: $\big[q_1(0),\ q_2(0),\ q_3(0)\big]^T = \big[0,\ 0,\ 0\big]^T$ degrees and $\big[\dot{q}_1(0),\ \dot{q}_2(0),\ \dot{q}_3(0)\big]^T = \big[0,\ 0,\ 0\big]^T$ degrees/sec.

The gains $K_p = \text{diag}\{k_{p1}, k_{p2}, k_{p3}\}$ and $K_v = \text{diag}\{k_{v1}, k_{v2}, k_{v3}\}$ for the hyperbolic control schemes must satisfy the condition (10) to prevent saturation of the actuators, which deteriorate the control system performance and leads the thermal and mechanical problems. Several trials were necessary in order to ensure a fast response of transient state, no oscillations, minimum overshoot and smaller steady-state error, and keep the actuators within their torque capabilities. For this purpose, guided by practical experience, from equation (10), we propose the following simple tuning rule: for the hyperbolic control gains $k_{pi}+k_{vi} < \frac{\tau_i^{\max} - k_{g_i}(\boldsymbol{q})}{\sqrt{n}\gamma_{m_p}}$; we have also considered incorporating $k_{g_i}(\boldsymbol{q})$ (see Property (2.8)). However, the derivative gain K_v must satisfy also the condition (19); this is, $\frac{\lambda_B^{\min}}{\sqrt{n}\gamma_{m_{vi}}} > \lambda_{K_v}^{\max} > 0$, where the $\lambda_B^{\min}$ is the eigenvalue of the matrix B. The robot parameters $k_{g_i}(\boldsymbol{q})$ and $\lambda_B^{\min}$ are available in [4].

For the PD control the proportional gains are tuned as $k_{pi} < \frac{\tau_i^{\max} - k_{g_i}(\boldsymbol{q})}{\tilde{q}_i(0)}$, and the derivative gains k_{vi} are tuning as $k_{vi} = \alpha_i k_{pi}$, where α_i is a unidimensional positive number $\in (0,\ 1)$, for $i = 1, 2, 3$. For all controllers, the tuning rules have been taken into account any initial position for $\tilde{q}_i(0)$ degrees and $\dot{q}_i(0) = 0\ \frac{\text{degrees}}{\text{sec}}$. The tunings used in the experimental results are listed in Table 4.

Note that cannot be identical gains for all controllers, because their mathematical structures are different, for the case of hyperbolic-type controllers as m increases, the peak value γ_m on the transient state also increases. For this reason, the same control gain values cannot be used for these controllers. Moreover, due to PD control structure has

Controller and tuning rule	Base joint	Shoulder joint	Elbow joint
Hyperbolic control for $m = 1, \boldsymbol{\tau}_{m1}$ $k_{pi} + k_{vi} < \frac{\tau_i^{\max} - k_{g_i}(\boldsymbol{q})}{\sqrt{3}}$ $\gamma_1 = 1$ $\frac{\lambda_B^{\min}}{\sqrt{3}\gamma_{m_1}} > \lambda_{K_v}^{\max} > 0$ $\lambda_B^{\min} = 0.406$ [Nm-rad/sec]	$k_{p1} = 28$ [Nm] $k_{v1} = 0.233$ [Nm] $\tau_1^{\max} = 50$ [Nm] $k_{g_1}(\boldsymbol{q}) = 0$ [Nm]	$k_{p2} = 60$ [Nm] $k_{v2} = 0.233$ [Nm] $\tau_2^{\max} = 150$ [Nm] $k_{g_2}(\boldsymbol{q}) = 40.28$ [Nm]	$k_{p3} = 5$ [Nm] $k_{v3} = 0.233$ [Nm] $\tau_3^{\max} = 15$ [Nm] $k_{g_3}(\boldsymbol{q}) = 1.81$ [Nm]
Hyperbolic control for $m = 2, \boldsymbol{\tau}_{m2}$ $k_{pi} + k_{vi} < \frac{\tau_i^{\max} - g_i(\boldsymbol{q})}{\sqrt{3}\ 1.05}$ $\gamma_2 = 1.05$ $\frac{\lambda_B^{\min}}{\sqrt{3}\gamma_{m_2}} > \lambda_{K_v}^{\max} > 0$ $\lambda_B^{\min} = 0.406$ [Nm-rad/sec]	$k_{p1} = 27$ [Nm] $k_{v1} = 0.223$ [Nm] $\tau_3^{\max} = 50$ [Nm] $k_{g_1}(\boldsymbol{q}) = 0$ [Nm]	$k_{p2} = 50$ [Nm] $k_{v1} = 0.223$ [Nm] $\tau_2^{\max} = 150$ [Nm] $k_{g_2}(\boldsymbol{q}) = 40.28$ [Nm]	$k_{p3} = 5$ [Nm] $k_{v3} = 0.223$ [Nm] $\tau_2^{\max} = 150$ [Nm] $k_{g_3}(\boldsymbol{q}) = 1.81$ [Nm]
Hyperbolic control for $m = 3, \boldsymbol{\tau}_{m3}$ $k_{pi} + k_{vi} < \frac{\tau_i^{\max} - g_i(\boldsymbol{q})}{\sqrt{3}\ 1.11}$ $\gamma_3 = 1.11$ $\frac{\lambda_B^{\min}}{\sqrt{3}\gamma_{m_3}} > \lambda_{K_v}^{\max} > 0$ $\lambda_B^{\min} = 0.406$ [Nm-rad/sec]	$k_{p1} = 25$ [Nm] $k_{v1} = 0.223$ [Nm] $\tau_1^{\max} = 50$ [Nm] $k_{g_1}(\boldsymbol{q}) = 0$ [Nm]	$k_{p2} = 50$ [Nm] $k_{v2} = 0.223$ [Nm] $\tau_2^{\max} = 150$ [Nm] $k_{g_2}(\boldsymbol{q}) = 40.28$ [Nm]	$k_{p3} = 5$ [Nm] $k_{v3} = 0.223$ [Nm] $\tau_3^{\max} = 15$ [Nm] $k_{g_3}(\boldsymbol{q}) = 1.81$ [Nm]
$\boldsymbol{\tau}_{PD}$ $k_{pi} < \frac{\tau_i^{\max} - k_{g_i}(\boldsymbol{q})}{\tilde{q}_i(0)}$ $k_{vi} = \alpha_i k_{pi}$ $0 < \alpha_i < 1$	$k_{p1} = 0.8 \left[\frac{\text{Nm}}{\text{degrees}}\right]$ $k_{v1} = 0.4 \left[\frac{\text{Nm-sec}}{\text{degrees}}\right]$ $\tau_1^{\max} = 50$ [Nm] $k_{g_1}(\boldsymbol{q}) = 0$ [Nm] $\alpha_3 = 0.5$	$k_{p2} = 2.5 \left[\frac{\text{Nm}}{\text{degrees}}\right]$ $k_{v2} = 0.75 \left[\frac{\text{Nm-sec}}{\text{degrees}}\right]$ $\tau_1^{\max} = 150$ [Nm] $k_{g_1}(\boldsymbol{q}) = 40.28$ [Nm] $\alpha_2 = 0.3$	$k_{p3} = 0.133 \left[\frac{\text{Nm}}{\text{degrees}}\right]$ $k_{v3} = 0.01 \left[\frac{\text{Nm-sec}}{\text{degrees}}\right]$ $\tau_1^{\max} = 50$ [Nm] $k_{g_2}(\boldsymbol{q}) = 1.81$ [Nm] $\alpha_3 = 0.06$

Tab. 2. Tuning rule for K_p and K_v gains.

a different mathematical form, the control gains adopt a different dimensional nature, which is reflected in their units.

Figure 3 contains the experimental results of position errors corresponding to three joints for the control τ_{m1}. Observe that each profile converges asymptotically to zero, after a smooth transient, all the components tend asymptotically to a small neighborhood of equilibrium point. The transient response of position errors not has oscillating, neither peak values or overshoot; in addition the robot's response achieving stationary-state times shorter than 1.4 sec. The position errors in steady-state have small values $\left[\tilde{q}_1(t),\ \tilde{q}_2(t),\ \tilde{q}_3(t)\right]^T = \left[-0.5774, 0.1272, -0.051\right]^T$ degrees, therefore its Euclidean norm for this time is $\|\tilde{\boldsymbol{q}}(t)\| = 0.5934$ degrees. The errors are present due to presence of static friction at the servomotors, however they are acceptably small.

Figure 4 shows the applied control torques $\boldsymbol{\tau}_{m1}$ for each joint, in steady-state some oscillations in the control signals are observed, but that behavior is not reflected in the response of position errors; this is due to the demanding hyperbolic damping effect to avoid the overshoot in closed-loop trajectories. From experimental results, it can be observed that, in agreement with the proposed tune-rule, all torque signals clearly evolve inside prescribed limits in Table 4.

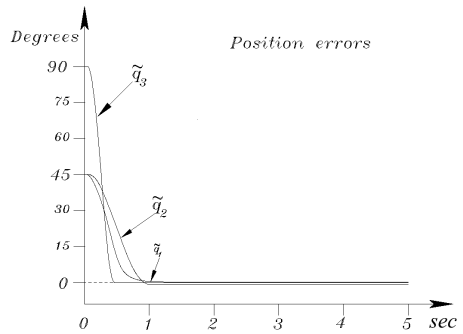

Fig. 3. Position errors of the hyperbolic controller when m=1.

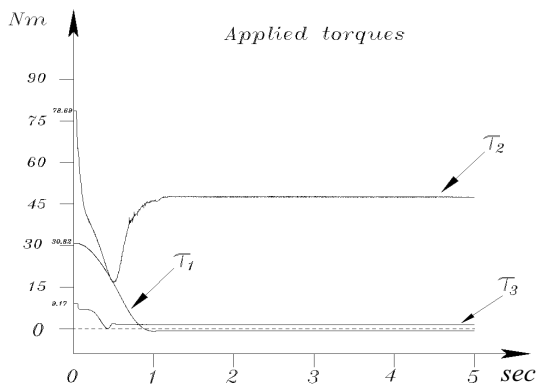

Fig. 4. Applied torques of the hyperbolic controller when $m = 1$.

The experimental results of position errors for the cases $\boldsymbol{\tau}_{m2}$ and $\boldsymbol{\tau}_{m3}$ are shown in Figures 5 and 7, respectively. It can be seen a fastest position errors response than the obtained for $\boldsymbol{\tau}_{m1}$; a minimum overshoot is observed for these cases (less than 0.04% with respect to the set-point q_{di}). All position errors converge faster to zero. For example, in $\boldsymbol{\tau}_{m2}$: the joint 1 at $t = 0.994$ sec, for joint 2 $t = 0.997$ sec, and joint 3 at $t = 0.929$ sec; The position errors in steady-state are $\big[\tilde{q}_1(t),\ \tilde{q}_2(t),\ \tilde{q}_3(t)\big]^T = \big[-0.1849,\ 0.4876,\ 0.1867\big]^T$ degrees. Therefore, the steady-state Euclidean norm is $\|\tilde{\boldsymbol{q}}(t)\| = 0.5539$ degrees. For the case $\boldsymbol{\tau}_{m3}$ the joint 1 at $t = 0.892$ sec reaches steady-state, joint 2 at $t = 0.923$ sec, and joint 3 $t = 0.867$ sec; the vector of position error $\tilde{\boldsymbol{q}}(t)$ in steady-state is $\big[\tilde{q}_1(t),\ \tilde{q}_2(t),\ \tilde{q}_3(t)\big]^T = \big[-0.3717,\ 0.3009,\ 0.2024\big]^T$ degrees. Thus, $\|\tilde{\boldsymbol{q}}(t)\| = 0.5193$ degrees.

The family of hyperbolic-type controllers has the ability to quickly drive the position error to zero when m increases its value, this feature is due to its exponential structure and the mathematics properties of the hyperbolic functions, the control $\boldsymbol{\tau}_m$ increases its

applied torque as high as is required, holding the actuator torque constraints through the tuning rule for the proportional and derivative K_v, then the transitory-state is fast and the vector de position errors $\tilde{\boldsymbol{q}}(t)$ reaches smaller values in steady-state while that, the servomotors are capable of holding the robot manipulator at rest at any desired joint positions vector $\boldsymbol{q}_d$.

Figures 6 and 8 show the applied torques corresponding to the algorithms $\boldsymbol{\tau}_{m2}$ and $\boldsymbol{\tau}_{m3}$, respectively. It can be observed that applied torques remain within the saturation limits supplied by servomotors of three joints. Observe that on transient-state of $\boldsymbol{\tau}_{m1}$, $\boldsymbol{\tau}_{m2}$ and $\boldsymbol{\tau}_{m3}$ there are switching effects or sign changes in the torque signals, this is due to the damping injection effect of the velocity joint $\dot{\boldsymbol{q}}$ within hyperbolic function structure of the derivative control action, therefore the vector of position errors $\tilde{\boldsymbol{q}}(t)$ reduces its magnitude, without over-impulses, neither oscillations or vibrations and because to properties of equilibrium point attractor, the vector of position errors converges asymptotically towards zero.

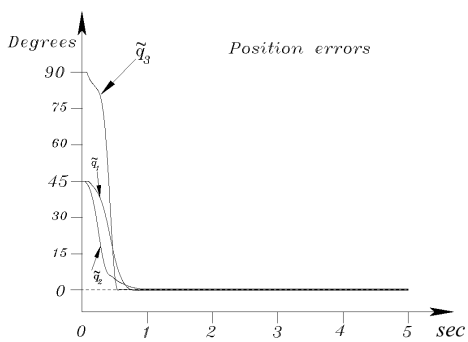

Fig. 5. Position errors of the hyperbolic controller when m=2.

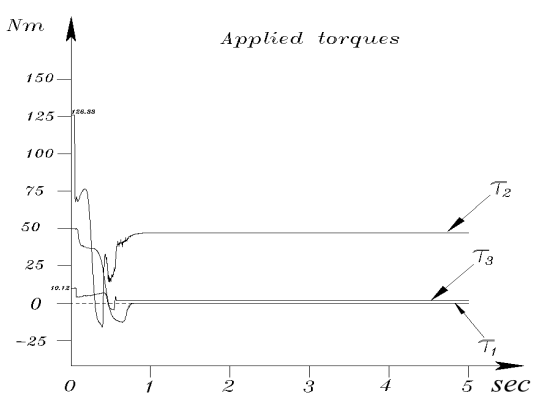

Fig. 6. Applied torques of the hyperbolic controller, case m=2.

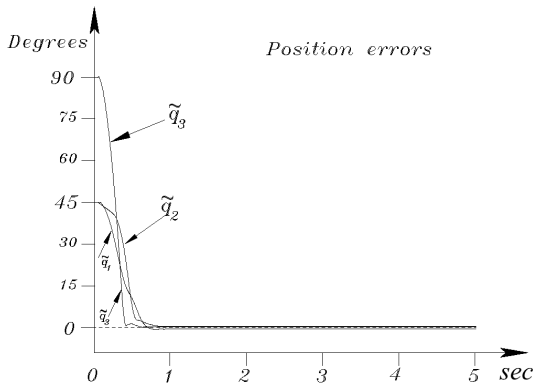

Fig. 7. Position errors of the hyperbolic controller, case m=3.

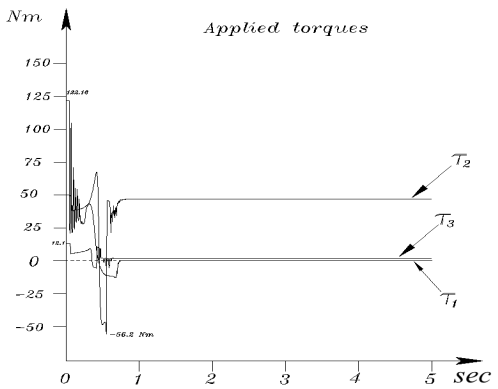

Fig. 8. Applied torques of the hyperbolic controller, case m=3.

Figures 9 and 10 present the position errors and applied torques, respectively for the control $\boldsymbol{\tau}_{PD}$. The tuning process of PD control gains K_p and K_v was complicated, and it not was easy, demanding much time, it depends of the user experience. Therefore, after making an effort, the tuning was achieved so that the robot's response was competitive with those obtained from the hyperbolic controllers. The combination of gains K_p and K_v leading to the best obtained PD control response with a good setting-time/overshoot.

It can be observed that the position errors arrive close to zero at $t = 1.14$ sec for joint 1, $t = 0.959$ sec for joint 2, and joint 3 at $t = 0.952$ sec. A smaller overshoot is observed and the steady-state positioning errors are large: $\left[\tilde{q}_1(t),\ \tilde{q}_2(t),\ \tilde{q}_3(t)\right]^T = \left[-0.2566,\ -0.7238,\ -0.8646\right]^T$ degrees. In fact, the steady-state Euclidean norm is $\|\tilde{\boldsymbol{q}}(t)\| = 1.1564$ degrees. In contrast with the hyperbolic control algorithms, which present the smaller position errors than $\tilde{\boldsymbol{q}}(t)$ of the $\boldsymbol{\tau}_{PD}$. The applied torques $\boldsymbol{\tau}_{PD}$ remain within the maximum torques supplied by servomotors. For the case of PD

controller, it was not possible to increase the derivative and proportional gains, because the saturation limits of the servomotors would be exceeded.

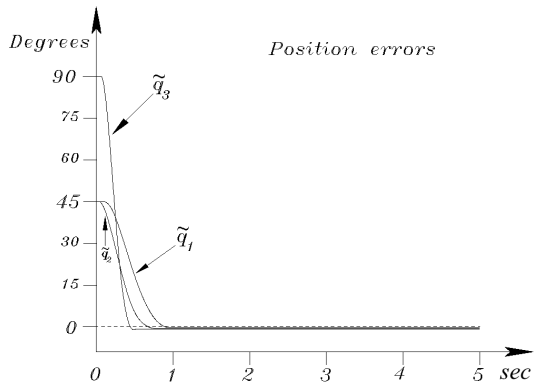

Fig. 9. Position errors of the PD control.

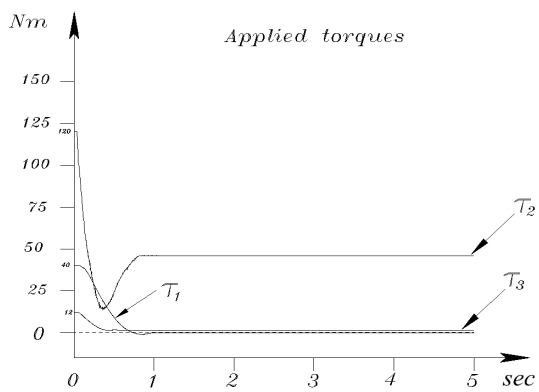

Fig. 10. Applied torque of the PD control.

The performance of evaluated control schemes was measurement to obtain faster transitory and steady response, both requirements must be satisfied simultaneously. The control objective is achieved avoiding input saturation for all experiments. We use scalar-valued $\mathcal{L}_2[\tilde{\boldsymbol{q}}(t)]$ norm as an objective numerical measure for the vector of position error [20]. The $\mathcal{L}_2[\tilde{\boldsymbol{q}}(t)]$ norm measures the root-mean-square of the $\tilde{\boldsymbol{q}}(t)$, it is given by

$$\mathcal{L}_2[\tilde{\boldsymbol{q}}(t)] \quad = \quad \sqrt{\frac{1}{T}\int_0^T \|\tilde{\boldsymbol{q}}(\sigma)\|^2 \mathrm{d}\sigma} \tag{20}$$

where $T \in \mathbb{R}_+$ represents the experimental time, for our experiments, it was $T = 5$ sec. The smaller $\mathcal{L}_2[\tilde{\boldsymbol{q}}(t)]$ means smaller position error $\tilde{\boldsymbol{q}}(t)$ and it is the best evaluated

controller performance.

The overall results are summarized in Figure 11, which includes the performance indexes of all evaluated controllers. The control algorithm $\boldsymbol{\tau}_{m1}$ has a $\mathcal{L}_2[\tilde{\boldsymbol{q}}_{(t)}]_{\boldsymbol{\tau}_{m1}} = 25.4006$ degrees, for $\boldsymbol{\tau}_{m2}$, $\mathcal{L}_2[\tilde{\boldsymbol{q}}_{(t)}]_{\boldsymbol{\tau}_{m2}}$ =24.6892 degrees, $\boldsymbol{\tau}_{m3}$ has $\mathcal{L}_2[\tilde{\boldsymbol{q}}_{(t)}]_{\boldsymbol{\tau}_{m3}}$ =23.4006 degrees, and for the PD controller $\mathcal{L}_2[\tilde{\boldsymbol{q}}_{(t)}]_{\boldsymbol{\tau}_{PD}}$ =27.8546 degrees. The performance of control scheme $\boldsymbol{\tau}_{m3}$ represents el 84% with respect to $\mathcal{L}_2[\tilde{\boldsymbol{q}}_{(t)}]_{\boldsymbol{\tau}_{PD}}$, this is the performance of $\boldsymbol{\tau}_{PD}$ is improved roughly 16% by $\boldsymbol{\tau}_{m3}$, 11.36% by $\boldsymbol{\tau}_{m2}$ and 8% by $\boldsymbol{\tau}_{m1}$. In general, the new family of bounded hyperbolic-type controllers showed better performance (smaller $\mathcal{L}_2[\tilde{\boldsymbol{q}}(t)]$) than the PD controller. Therefore, the usefulness of proposed methodology can be concluded and it represents an attractive solution for industrial applications, process automation and manufacturing systems.

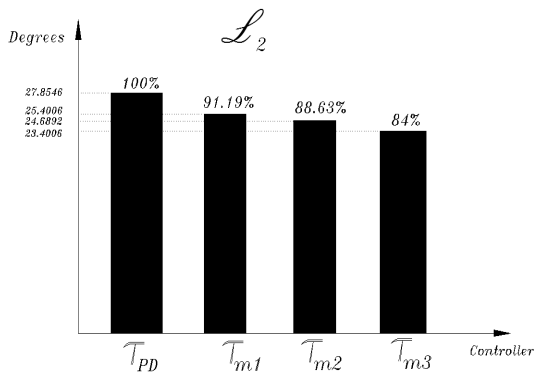

Fig. 11. Performance indexes of evaluated controllers.

Remark I. Note that input signal constraint (9) is very strict, due to its hyperbolic exponential structure and the tuning of its gains, then to guarantee that it can be practiced in all real scenarios, the proposed control (6) requires convergence of internal signals in the servodrivers of the robot [10]; additional, it can handle uncertain nonlinear electrically driven robots in the presence of external disturbances [11]. Therefore is better to guarantee asymptotically convergence of the closed-loop equation (11), and the torque signals is bounded. The proposed control (6) helps to generate an asymptotically stable attractor in overall closed-loop system (11), this means that it makes immune to any initial condition $\left[\tilde{\boldsymbol{q}}(0), \dot{\boldsymbol{q}}(0)\right]^T \in \mathbb{R}^{2n}$ into attractor region.

Another important aspect to consider is about tuning of the gains, which is limited by practical considerations on the torque saturation in the servomotors. To overcome this problem, we have proposed a simple tuning-rule, which is easy to find adequate gains, a design guidelines without regard to initial conditions to tune the controller gains is described by (10), guaranteeing that the demanded torques remain inside the prescribed

limits (see Table 2). From experimental results in agreement with the proposed tune-rule (10), all torque signals clearly evolve inside prescribed limits provided in Table 1. In this way the control signal (6) is a suitable signal for the internal convergence inside the servoactuators.

Remark II. As further research is possible to carry out the extension of the control family proposed for the tracking problem or motion control, which is much more complicated than regulation. We propose the following control structure:

$$\boldsymbol{\tau} = K_p \begin{bmatrix} \frac{\sinh^{2m-1}(\tilde{q}_1)\cosh(\tilde{q}_1)}{1+\sinh^{2m}(\tilde{q}_1)} \\ \frac{\sinh^{2m-1}(\tilde{q}_2)\cosh(\tilde{q}_2)}{1+\sinh^{2m}(\tilde{q}_2)} \\ \vdots \\ \frac{\sinh^{2m-1}(\tilde{q}_n)\cosh(\tilde{q}_n)}{1+\sinh^{2m}(\tilde{q}_n)} \end{bmatrix} + K_v \begin{bmatrix} \frac{\sinh^{2m-1}(\dot{\tilde{q}}_1)\cosh(\dot{\tilde{q}}_1)}{1+\sinh^{2m}(\dot{\tilde{q}}_1)} \\ \frac{\sinh^{2m-1}(\dot{\tilde{q}}_2)\cosh(\dot{\tilde{q}}_2)}{1+\sinh^{2m}(\dot{\tilde{q}}_2)} \\ \vdots \\ \frac{\sinh^{2m-1}(\dot{\tilde{q}}_n)\cosh(\dot{\tilde{q}}_n)}{1+\sinh^{2m}(\dot{\tilde{q}}_n)} \end{bmatrix} + M(\boldsymbol{q})\ddot{\boldsymbol{q}}_d + C(\boldsymbol{q},\dot{\boldsymbol{q}})\dot{\boldsymbol{q}}_d + \boldsymbol{g}(\boldsymbol{q}) + B\dot{\boldsymbol{q}}_d \quad (21)$$

where $m \in N$ is a positive integer number, $\tilde{\boldsymbol{q}}$ is the $n \times 1$ vector of joint tracking error, which is defined as $\tilde{\boldsymbol{q}} = \boldsymbol{q}_d(t) - \boldsymbol{q}$, being $\boldsymbol{q}_d(t)$ the time-varying desired position trajectory; $\dot{\tilde{\boldsymbol{q}}}$ is the $n \times 1$ vector of joint velocity error defined as $\dot{\tilde{\boldsymbol{q}}} = \dot{\boldsymbol{q}}_d(t) - \dot{\boldsymbol{q}}$; the desired velocity and desired acceleration trajectories are $\dot{\boldsymbol{q}}_d(t)$ and $\ddot{\boldsymbol{q}}_d(t)$, respectively; $K_p, K_v \in \mathbb{R}^{n\times n}$ are positive definite diagonal matrices. Note that, if $\boldsymbol{q}_d$ is a constant vector (set-point), then control structure (21) becomes the regulator (6). It is clear that to implement the trajectory control it is necessary to know the numerical value of its parameters, which is resolved with parametric identification. With a generalization of the strict Lyapunov function (12) is possible to obtain the global asymptotic convergence of the state variables $\left[\tilde{\boldsymbol{q}}(t),\ \dot{\tilde{\boldsymbol{q}}}(t)\right]^T$ to the equilibrium point $\mathbf{0} \in \mathbb{R}^{2n}$.

5. CONCLUSIONS

In this paper, we have presented a family of bounded hyperbolic-type control algorithms to solve the position control problem. When the exponent m increases, the hyperbolic-type controllers have a short transient state and smaller steady-state position errors, the suitable combination of hyperbolic functions has characteristic to quickly drive the position error to zero, this feature is due to its exponential structure and hyperbolic mathematics properties.

Our propose is supported by a rigorous asymptomatically stability analysis in sense Lyapunov's stability, we have proposed a strict Lyapunov function to establish conditions for ensuring global regulation. Through the satisfaction of simple inequalities on the saturation function bounds, the global regulation is achieved, and therefore, the global regulation objective is proved, avoiding saturation in the control signals; this ensures that the equilibrium point of the closed-loop dynamics is globally asymptotically stable.

The tuning procedure for proportional and derivative gains is sufficient to select both gains to satisfy simple inequalities on bounds of saturation, the actual choice depends on practical considerations of torque saturation in the servomotors. However, in contrast for the PD control gains control, their tuning was very complicated. The performance of evaluated control schemes was measurement to obtain faster transitory and steady response, both requirements must be satisfied simultaneously. The control objective is

achieved avoiding input saturation for all experiments. In this sense, the experiments confirm the proposed methodology is suitable for applications of position control.

The proposed family permits the implementation of large number of hyperbolic-type control structures with potential applications at the industrial sector; and opening new control design possibilities to improve their closed-loop behavior.

ACKNOWLEDGEMENT

This work was partially supported by Group Project "Control de Posición con Ganancias Variables de Robots Manipuladores", 100048866-VIEP2019 BUAP. México.

(Received May 23, 2018)

REFERENCES

[1] E. Aguiñaga. A. Zavala, V. Santibañez, and F. Reyes: Global trajectory tracking through static feedback for robot manipulators with bounded inputs. IEEE Trans. Control Systems Technol. *17* (2009), 4, 934–944. DOI:10.1109/tcst.2009.2013938

[2] R. J. Caverly, D. E. Zlotink, L. J. Bridgeman, and J. R. Fobres: Saturated proportional derivative control of a single-link flexible-joint manipulator. Robotics computer-Integrated Manufact. *30* (2014), 658–666. DOI:10.1016/j.rcim.2014.06.001

[3] R. J. Caverly, D. E. Zlotink, and J. R. Forbes: Saturated control of flexible-joint manipulators using a Hammerstein strictly positive real compensator. Robotica *34* (2014), 1367–1382. DOI:10.1017/s0263574714002343

[4] C. Chavez-Olivares, F. Reyes-Cortes, E. Gonzalez-Galvan, M. Mendoza-Gutierrez, and I. Bonilla-Gutierrez: Experimental evaluation of parameter identification on an anthropomorphic direct drive robot. Int. J. Advanced Robotic Systems *9* (2012), 4, 1–18. DOI:10.5772/52190

[5] J. Craig, P. Hsu, and S. Sastry: Adaptive control of mechanical manipulators. Int. J. Robotics Research *6* (1987), 2, 16–28. DOI:10.1177/027836498700600202

[6] A. del Petre: Joint position and velocity bounds in discrete-time acceleration/torque control of robot manipulators. IEEE Robotics Automat. Lett. *3* (2018), 1, 281—288. DOI:10.1109/lra.2017.2738321

[7] N. Fischer, A. Dani, N. Sharma, and W. Dixon: Saturated control of an uncertain nonlinear system with input delay. Automatica *49* (2013), 1741–1747. DOI:10.1016/j.automatica.2013.02.013

[8] N. Fischer, Z. Kan, R. Kamalapurkar, and W. Dixon: Saturated RISE feedback control for a class of second-order nonlinear systems. IEEE Trans. Automat. Control *59* (2014), 4, 1094–1099. DOI:10.1109/tac.2013.2286913

[9] A. Izadbakhsh and P. Kheirkhahan: Nonlinear PID control of electrical flexible joint robots-Theory and experimental verification. In: 2018 IEEE International Conference on Industrial Technology (ICIT), Lyon 2018, pp. 250–255. DOI:10.1109/icit.2018.8352185

[10] A. Izadbakhsh and M. M. Fateh: Real-time robust adaptive control of robots subjected to actuator voltage constraint. Nonlinear Dynamics, Springer *78* (2014) 3, 1999–2014. DOI:10.1007/s11071-014-1574-z

[11] A. Izadbakhsh and P. Kheirkhahan: On the voltage-based control of robot manipulators revisited. Int. J. Control, Automat. Systems *16* (2018), 4, 1887–1894. DOI:10.1007/s12555-017-0035-0

[12] R. Kelly and V. Santibañez: Global regulation of elastic joint robots based on energy shaping. IEEE Trans. Automat. Control *43* (1998), 10, 1451–1456. DOI:10.1109/9.720506

[13] R. Kelly, V. Santibañez, and A. Loria: Control of Robot Manipukators in Joint Space. Springer, 2005. DOI:10.1002/rnc.1114

[14] D. Lopez, A. Loria, and A. Zavala: Adaptive tracking control of Euler–Lagrange systems with bounded controls. Int. J. Adaptive Control Signal Process. *31* (2017), 299–313. DOI:10.1002/acs.2697

[15] M. Mendoza, I. Bonilla, F. Reyes, and E. Gonzalez-Galvan: A Lyapunov-based design tool of impedance controllers for robot manipulators. Kybernetika *48* (2012), 6, 1136–1155.

[16] M. Mendoza, A. Zavala-Rao, V. Santibanez, and F. Reyes: Output-feedback proportional-integral-derivative-type control with simple tuning fot the global regulation of robot manipulators with input constraints. IET Control Theory Appl. Inst. Engrg. Technol. *10000* (2015), 1–10. DOI:10.1049/iet-cta.2014.0680

[17] J. Moreno and V. Santibañez: Robust saturated pi joint velocity control for robot manipulators. Asian J. Control *15* (2013), 1, 64–79. DOI:10.1002/asjc.586

[18] J. Orrante, V. Santibañez, and M. Hernandez: A new tuning procedure for nonlinear PID global regulators with bounded— torques for rigid robots. Robotica *33* (2015), 4, 1926–1947. DOI:10.1017/s0263574714001131

[19] J. A. Ramirez, V. Santibañez, and R. Campa: Stability of robot manipulators under saturated PID compensation. IEEE Trans. Control Systems Technol. *16* (2008), 6, 1333–1341. DOI:10.1109/tcst.2008.917875

[20] F. Reyes, J. Cid, M. A. Limon, and M. Cervantes: Square root-type control for robot manipulators. Int. J. Advanced Robotic Systems *10* (2013), 39, 1–7. DOI:10.5772/52500

[21] M. C. Rodriguez, I. Bonilla, M. Mendoza, and C. Chavez: Saturating stiffness control of robot manipulators with bounded inputs. Int. J. Appl. Math. Computer Sci. *27* (2017), 1, 79–90. DOI:10.1515/amcs-2017-0006

[22] J. G. Romero, R. Ortega, and A. Donaire: Robust energy shaping control of mechanical systems. Systems Control Lett. *62* (2016), 770–780. DOI:10.1016/j.sysconle.2013.05.011

[23] V. Santibañez, R. Kelly, and F. Reyes: A new set-point controller with bounded torques for robot manipulators. IEEE Trans. Industr. Electron. *45* (1998), 1, 126–133. DOI:10.1109/41.661313

[24] V. Santibañez, R. Kelly, and M. A. Llama: A novel global asymptotic stable set-point fuzzy controller with bounded torques for robot manipulators. IEEE Trans. Fuzzy Systems *13* (2005), 3, 362–372. DOI:10.1109/tfuzz.2004.841735

[25] K. Shojaei and A. Chatraei: A saturating extension of an output feedback controller for internally damped Euler–Lagrange systems. Asian J. Control *17* (2015), 6, 2175–2187. DOI:10.1002/asjc.1115

[26] B. Siciliano, L. Sciavicco, L. Villani, and G. Oriolo: Robotics: Modelling, Planning and Control. Springer Publishing Company, Incorporated, 2010.

[27] B. Siciliano and O. Kathib: Handbook of Robotics. Second Edition. Springer, 2016. DOI:10.1007/978-3-319-32552-1_1

[28] M. W. Spong, S. Hutchinson, and M. Vidyasagar: Robot Modeling and Control. John Wiley and Sons, Inc., 2006. DOI:10.1108/ir.2006.33.5.403.1

[29] Y. Su, P. C. Muller, and C. Zheng: Global asymptotic saturated PID Control for robot manipulators. IEEE Trans. Control Systems Technol. *18* (2010), 6, 1280–1288. DOI:10.1109/tcst.2009.2035924

[30] D. Sun, S. Hu, X. Shao, and C. Liu: Global stability of a saturated nonlinear PID controller for robot manipulators. IEEE Trans. Control Systems Technol. *17* (2009), 4, 892–899. DOI:10.1109/tcst.2008.2011748

[31] M. Takegaki and S. Arimoto: A new feedback method for dynamic control of manipulators. ASME J. Dyn. Syst. Meas. Control *103* (1981), 119–125. DOI:10.1115/1.3139651

[32] A. Yarza, V. Santibañez, and J. Moreno: Global asymptotic stability of the classical PID controller by considering saturation effects in industrial robots. Int. J. Advanced Robotic Systems *8* (2011), 4, 34–42. DOI:10.5772/45688

[33] A. Zavala, M. Mendoza, V. Santibañez, and F. Reyes: Output-feedback proportional-integral-derivative-type control with multiple saturating structure for the global stabilization of robot manipulators with bounded inputs. Int. J. Advanced Robotic Systems *6* (2016), 1–12. DOI:10.1177/1729881416663368

[34] A. Zelei, L. Bencsik, and G. Stepan: Handling Actuator Saturation As Underactuation: Case study with acroboter service robot. J. Computat. Nonlinear Dynamics *12* (2016), 3, 031011–031015. DOI:10.1115/1.4034868

Fernando Reyes-Cortes, 18 Sur y Av. San Claudio, Col. San Manuel C. U., Puebla 72570, México. Edificio FCE6, Laboratorio de Robótica y Control, Facultad de Ciencias de la Electrónica, Benemérita Universidad Autónoma de Puebla. México.
e-mail: fernando.reyes@correo.buap.mx

Olga Felix-Beltran, 18 Sur y Av. San Claudio, Col. San Manuel C. U., Puebla 72570, México. Edificio FCE6, Laboratorio de Robótica y Control, Facultad de Ciencias de la Electrónica, Benemérita Universidad Autónoma de Puebla. México.
e-mail: olga.felix@correo.buap.mx

Jaime Cid-Monjaraz, 18 Sur y Av. San Claudio, Col. San Manuel C. U., Puebla 72570, México. Edificio FCE6, Laboratorio de Robótica y Control, Facultad de Ciencias de la Electrónica, Benemérita Universidad Autónoma de Puebla. México.
e-mail: jaime.cid@correo.buap.mx

Gweni Alonso-Aruffo, 26 Rue de l' Epitaphe- CS 51813 – 25030 Besancon Cedex, France, Ecole Nationale Supérieure de Mécanique et des Microtechniques. France.
e-mail: gweni.alonso@laposte.net